2. Uchiyama T, Yodoi J, Sagawa K, Takatsuki K, Uchino H. Adult T-cell leukemia: clinical and hematologic features of 16 cases. Blood 1977;50:481–92.
3. Poiesz BJ, Ruscetti FW, Gazdar AF, Bunn PA, Minna JD, Gallo RC. Detection and isolation of type C retrovirus particles from fresh and cultured lymphocytes of a patient with cutaneous T-cell lymphoma. Proc Natl Acad Sci USA 1980;77:7415–9.
4. Wong-Staal F, Gallo RC. Human T-lymphotropic retroviruses. Nature (Lond) 1985; 317:395–403.
5. Arisawa K, Soda M, Endo S, et al. Evaluation of adult T-cell leukemia/lymphoma incidence and its impact on non-Hodgkin lymphoma incidence in southwestern Japan. Int J Cancer 2000;85:319–24.
6. Yoshida M. Multiple viral strategies of HTLV-1 for dysregulation of cell growth control. Annu Rev Immunol 2001;19 475–96.
7. Franchini G, Fukumoto R, Fullen JR. T-cell control by human T-cell leukemia/ lymphoma virus type 1. Int J Hematol 2003;78:280–96.
8. Jeang KT. Functional activities of the human T-cell leukemia virus type I Tax oncoprotein: cellular signaling through NF-kappa B. Cytokine Growth Factor Rev 2001;12:207–17.
9. Fujii M, Tsuchiya H, Chuhjo T, Akizawa T, Seiki M. Interaction of HTLV-1 Tax1 with p67SRF causes the aberrant induction of cellular immediate early genes through CArG boxes. Genes Dev 1992;6:2066–76.
10. Kwok RP, Laurance ME, Lundblad JR, et al. Control of cAMP-regulated enhancers by the viral transactivator Tax through CREB and the co-activator CBP. Nature (Lond) 1996;380:642–6.
11. Jeang KT, Widen SG, Semmes OJ 4th, Wilson SH. HTLV-I trans-activator protein, tax, is a trans-repressor of the human beta-polymerase gene. Science (Wash D C) 1990;247:1082–4.
12. Suzuki T, Uchida-Toita M, Yoshida M. Tax protein of HTLV-1 inhibits CBP/p300-mediated transcription by interfering with recruitment of CBP/p300 onto DNA element of E-box or p53 binding site. Oncogene 1999;18:4137–43.
13. Jin DY, Spencer F, Jeang KT. Human T cell leukemia virus type 1 oncoprotein Tax targets the human mitotic checkpoint protein MAD1. Cell 1998;93:81–91.
14. Takeda S, Maeda M, Morikawa S, et al. Genetic and epigenetic inactivation of tax gene in adult T-cell leukemia cells. Int J Cancer 2004;109:559–67.
15. Tamiya S, Matsuoka M, Etoh K, et al. Two types of defective human T-lymphotropic virus type I provirus in adult T-cell leukemia. Blood 1996;88:3065–73.
16. Furukawa Y, Kubota R, Tara M, Izumo S, Osame M. Existence of escape mutant in HTLV-I tax during the development of adult T-cell leukemia. Blood 2001;97:987–93.
17. Koiwa T, Hamano-Usami A, Ishida T, et al. 5'-long terminal repeat-selective CpG methylation of latent human T-cell leukemia virus type 1 provirus in vitro and in vivo. J Virol 2002;76:9389–97.
18. Bangham CR. Human T-lymphotropic virus type 1 (HTLV-1): persistence and immune control. Int J Hematol 2003;78:297–303.
19. Sakashita A, Hattori T, Miller CW, et al. Mutations of the p53 gene in adult T-cell leukemia. Blood 1992;79:477–80.
20. Hatta Y, Hirama T, Miller CW, Yamada Y, Tomonaga M, Koeffler HP. Homozygous deletions of the p15 (MTS2) and p16 (CDKN2/MTS1) genes in adult T-cell leukemia. Blood 1995;85:2699–704.
21. Nosaka K, Maeda M, Tamiya S, Sakai T, Mitsuya H, Matsuoka M. Increasing methylation of the CDKN2A gene is associated with the progression of adult T-cell leukemia. Cancer Res 2000;60:1043–8.
22. Costello JF, Fruhwald MC, Smiraglia DJ, et al. Aberrant CpG-island methylation has non-random and tumour-type-specific patterns. Nat Genet 2000;24:132–8.
23. Esteller M, Corn PG, Baylin SB, Herman JG. A gene hypermethylation profile of human cancer. Cancer Res 2001;61:3225–9.
24. Hayashizaki Y, Hirotsune S, Okazaki Y, et al. Restriction landmark genomic scanning method and its various applications. Electrophoresis 1993;14:251–8.
25. Gonzalgo ML, Liang G, Spruck CH, 3rd, Zingg JM, Rideout WM, 3rd, Jones PA. Identification and characterization of differentially methylated regions of genomic DNA by methylation-sensitive arbitrarily primed PCR. Cancer Res 1997;57:594–9.
26. Ushijima T, Morimura K, Hosoya Y, et al. Establishment of methylation-sensitive-representational difference analysis and isolation of hypo- and hypermethylated genomic fragments in mouse liver tumors. Proc Natl Acad Sci USA 1997;94:2284–9.
27. Huang TH, Laux DE, Hamlin BC, Tran P, Tran H, Lubahn DB. Identification of DNA methylation markers for human breast carcinomas using the methylation-sensitive restriction fingerprinting technique. Cancer Res 1997;57:1030–4.
28. Toyota M, Ho C, Ahuja N, et al. Identification of differentially methylated sequences in colorectal cancer by methylated CpG island amplification. Cancer Res 1999;59: 2307–12.
29. Ballestar E, Paz MF, Valle L, et al. Methyl-CpG binding proteins identify novel sites of epigenetic inactivation in human cancer. EMBO J 2003;22:6335–45.
30. Yoshida M, Nosaka K, Yasunaga J, Nishikata I, Morishita K, Matsuoka M. Aberrant expression of the MEL1S gene identified in association with hypomethylation in adult T-cell leukemia cells. Blood 2004;103:2753–60.
31. OhYama T, Tsukumo S, Yajima N, Sakamaki K, Yonehara S. Reduction of thymocyte numbers in transgenic mice expressing viral FLICE-inhibitory protein in a Fas-independent manner. Microbiol Immunol 2000;44:289–97.
32. Krueger A, Schmitz I, Baumann S, Krammer PH, Kirchhoff S. Cellular FLICE-inhibitory protein splice variants inhibit different steps of caspase-8 activation at the CD95 death-inducing signaling complex. J Biol Chem 2001;276:20633–40.
33. Xiong Z, Laird PW. COBRA: a sensitive and quantitative DNA methylation assay. Nucleic Acids Res 1997;25:2532–4.
34. Clark SJ, Harrison J, Paul CL, Frommer M. High sensitivity mapping of methylated cytosines. Nucleic Acids Res 1994;22:2990–7.
35. Takai D, Jones PA. Comprehensive analysis of CpG islands in human chromosomes 21 and 22. Proc Natl Acad Sci USA 2002;99:3740–5.
36. Palmisano WA, Crume KP, Grimes MJ, et al. Aberrant promoter methylation of the transcription factor genes PAX5 alpha and beta in human cancers. Cancer Res 2003;63:4620–5.
37. Cameron EE, Bachman KE, Myohanen S, Herman JG, Baylin SB. Synergy of demethylation and histone deacetylase inhibition in the re-expression of genes silenced in cancer. Nat Genet 1999;21:103–7.
38. Mittelstadt PR, Ashwell JD. Cyclosporin A-sensitive transcription factor Egr-3 regulates Fas ligand expression. Mol Cell Biol 1998;18:3744–51.
39. Krammer PH. CD95's deadly mission in the immune system. Nature (Lond) 2000; 407:789–95.
40. Shields JM, Christy RJ, Yang VW. Identification and characterization of a gene encoding a gut-enriched Kruppel-like factor expressed during growth arrest. J Biol Chem 1996;271:20009–17.
41. Segre JA, Bauer C, Fuchs E. Klf4 is a transcription factor required for establishing the barrier function of the skin. Nat Genet 1999;22:356–60.
42. Zhang W, Geiman DE, Shields JM, et al. The gut-enriched Kruppel-like factor (Kruppel-like factor 4) mediates the transactivating effect of p53 on the p21WAF1/ Cip1 promoter. J Biol Chem 2000;275:18391–8.
43. Yoon HS, Chen X, Yang VW. Kruppel-like factor 4 mediates p53-dependent G1/S cell cycle arrest in response to DNA damage. J Biol Chem 2003;278:2101–5.
44. Yoon HS, Yang VW. Requirement of Kruppel-like factor 4 in preventing entry into mitosis following DNA damage. J Biol Chem 2004;279:5035–41.
45. Etoh K, Tamiya S, Yamaguchi K, et al. Persistent clonal proliferation of human T-lymphotropic virus type I-infected cells in vivo. Cancer Res 1997;57:4862–7.
46. Issa JP. Age-related epigenetic changes and the immune system. Clin Immunol 2003;109:103–8.

Transcriptional repression of the *p15* gene predicts the clinical outcome of acute myeloblastic leukemia with intermediate and adverse cytogenetics

Leukemia (2004) **18**, 1146–1148. doi:10.1038/sj.leu.2403362
Published online 15 April 2004

TO THE EDITOR

In acute myeloblastic leukemia (AML), cytogenetic abnormalities are one of the most important factors predicting the clinical outcome. However, more than 40% of patients with *de novo* AML have a normal karyotype, and therefore lack informative cytogenetic markers. The intermediate or adverse cytogenetic risk group includes a heterogeneous cohort of patients, and little is known about the underlying molecular mechanisms contributing to the clinical heterogeneity. To date, several molecular abnormalities have been examined for their clinical significance in AML. For example, internal tandem duplications (ITDs) in the receptor tyrosine kinase *FLT3* gene, which are observed in approximately 20% of AML, are associated with an unfavorable clinical outcome. On the other hand, mutations in the transcription factor C/EBPα were seen in about 10% of AML patients and are associated with a favorable clinical outcome. Intriguingly, mutations of these genes were frequently seen in patients with a normal karyotype. Since a considerable number of patients with AML do not have these genetic abnormalities, it is of importance to clarify the clinical significance of further molecular alterations.

Hypermethylation of the *p15* gene has been demonstrated in more than 60% of patients with AML, while alteration of the *p16* gene and homozygous deletion of the *p15* gene were rarely observed.[1–3] However, only a few studies have reported the relationship between *p15* methylation and clinical outcome in AML. A trend toward shorter survival was observed among the relatively small numbers of patients with adult AML in whom the *p15* gene was methylated.[3] In AML M3, *p15* methylation and no *p15* mRNA expression correlated with shorter disease-free survival (DFS).[4] The clinical significance of *p15* inactivation largely remains to be determined, although frequent hypermethylation of the *p15* gene was selectively observed in AML.

In addition, most analyses of CpG island hypermethylation of the *p15* gene employ techniques capable of studying only a few CpG sites within the CpG island, such as Southern blotting analysis using methylation-sensitive restriction enzymes or methylation-specific polymerase chain reaction (PCR). Recent studies of *p15* methylation using bisulfite genomic sequencing of whole CpG sites have revealed the pronounced heterogeneity of *p15* methylation between individual alleles. The methylation density of the *p15* CpG island was correlated with mRNA expression, as analyzed by reverse transcriptase–PCR (RT-PCR).[5] Since RT-PCR is not a quantitative method, we thought that a more quantitative analysis of expression was needed to evaluate the silencing of the *p15* gene caused by various degrees of methylation. In this study, we established real-time quantitative RT-PCR (RQ-PCR) and examined whether the level of *p15* mRNA expression is associated with clinical outcome in AML patients.

We examined bone marrow mononuclear cells (BMMCs) from 108 Japanese patients with *de novo* AML. BMMCs from 10 patients with malignant lymphoma lacking BM involvement were also examined. Each patient gave informed consent for use of their samples according to guidelines based on the tenets of the revised Helsinki Protocol by the Institutional Committees for the Protection of Human Subjects and Analysis of the Human Genome. Patients were treated with intensive chemotherapy based on the Japan Adult Leukemia Study Group multicenter protocols in the AML87, AML89, AML92 and AML95 studies. For the *p15* standard plasmid, 451 bp fragments were amplified using primers spanning exons 1 and 2 of the *p15* gene to avoid amplification of genomic sequences. For the *GAPDH* standard plasmid, primers were designed to amplify 545 bp fragments of the *GAPDH* gene from the sequences of different exons. The sequences of primers were as follows: p15WS5, 5′-TGGGGGCGGCAGCGATGAG-3′ (357–375) and p15WAS5, 5′-AGGTGGGTGGGGGTGGGAAAT-3′ (807–787) for *p15*, and gapLS, 5′-GGAGCCAAAAGGGTCATCATCT-3′ (418–439) and gapLA, 5′-TCAAAGGTGGAGGAGTGGGTGT-3′ (962–941) for *GAPDH*, where the numbers in the parentheses were based on published sequences available from GenBank under Accession Nos. L36844 (p15) and NM_002046 (GAPDH). The PCR products were subcloned into the plasmid pGEM-T Easy Vector (Promega, Madison, WI, USA). Molecular concentrations were calculated and serial dilutions of the standard plasmid were prepared. We designed primers and the TaqMan probe for *p15* RQ-PCR, which produced 169 bp PCR fragments spanning exons 1 and 2, to avoid amplification of *p16* mRNA whose exon 2 is highly homologous to the *p15* gene. We also designed primers and a probe for *GAPDH* RQ-PCR, which amplified 101 bp PCR fragments, using the Primer-Express Software (Applied Biosystems, Foster City, CA, USA). The sequences of primers and probes for RQ-PCR were as follows: p15WS3, 5′-GGACTAGTGGAGAAGGTGCG-3′ (397–416), p15WAS, 5′-TGAGAGTGGCAGGGTCT-3′ (565–549) and 5′-(FAM)-CGCGGATCCCAACGGAGTCAACC-(TAMRA)-3′ (435–457) for *p15*, and gapSF, 5′-ACCAACTGCTTAGCACCCCT-3′ (535–554), gapSR, 5′-GTCTTCTGGGTGGCAGTGAT-3′ (635–616) and 5′-(FAM)-CTTTGGTATCGTGGAAGGACTCATGACC-(TAMRA)-3′ (576–603) for *GAPDH*. To correct for differences in the RNA quantity, we calculated the ratio of the copy numbers of *p15* and *GAPDH* mRNA transcripts in a given sample. Amplification and data analysis were carried out using the ABI PRISM 7700 Sequence Detection System (Applied Biosystems). All samples were examined in duplicate. Bisulfite genomic sequencing confirmed that the methylation density well correlated with *p15* mRNA expression (unpublished data). In order to classify the AML samples according to the *p15* expression level, we assumed that mean values below 2 SEs of the control BM samples were low *p15* expression levels, and the others were high expression levels. Mutations of the *FLT3* gene were also examined as previously described.[6]

The levels of *p15* mRNA expression according to cytogenetic risk groups and FLT3 mutations are summarized in Table 1. Of

Correspondence: Dr N Asou, Department of Internal Medicine II, Kumamoto University School of Medicine, 1-1-1 Honjo, Kumamoto 860-8556, Japan; Fax: +81 96 363 5265;
E-mail: ktcnasou@kaiju.medic.kumamoto-u.ac.jp
Received 20 September 2003; accepted 12 February 2004; Published online 15 April 2004

40 patients with favorable cytogenetics, 26 (65%) showed low *p15* expression. On the other hand, 34 of the 68 (50%) remaining patients with either intermediate, adverse or undetermined cytogenetics had low *p15* expression ($P=0.13$). There was no appreciable difference between *p15* expression levels and ITDs or D835 mutations in the *FLT3* gene. The clinical outcome in 98 patients with AML who received intensive chemotherapy was examined according to the *p15* expression level. Remaining 10 patients who received supportive therapy only or mild chemotherapy because of older age or poor clinical condition were excluded from this analysis. No statistical significance was observed between the *p15* expression level and the complete remission rate in 98 AML patients.

Table 1 Relationships between the level of *p15* mRNA expression and cytogenetic risk group or FLT3 mutation

		Level of p15 mRNA expression	
	Total	*Low*	*High*
No. of patients	108	60	48
Cytogenetics (MRC criteria)			
Favorable	40	26	14
t(8;21)	15	10	5
t(15;17)	14	12	2
inv(16)	11	4	7
Intermediate	50	25	25
Normal	31	16	15
Others	19	9	10
Adverse	7	4	3
Undetermined	11	5	6
FLT3 mutation			
ITD	14	8	6
D835	11	5	6

ITD: internal tandem duplication, D835: missense mutation at the D835 in the *FLT3* gene.

Patients with favorable cytogenetics consisting of t(8;21), t(15;17) and inv(16), which were confirmed by RT-PCR analysis, showed significantly longer survival than those with intermediate or adverse cytogenetics according to the MRC criteria ($P=0.039$) (Figure 1a). In univariate analysis, there were no significant differences between the *p15* expression level and DFS, event-free survival (EFS), or overall survival (OS) (Figure 1b and data not shown). A total of 38 patients with favorable cytogenetics had no differences between the *p15* expression level and DFS, EFS, or OS ($P=0.82$, 0.79, 0.95, respectively). Since 11 patients with undetermined cytogenetics were neither M2 with t(8;21), M3 with t(15;17), nor M4Eo with inv(16) by morphological and RT-PCR analyses, we included these patients in the intermediate or adverse cytogenetic risk group. Among the patients with intermediate or adverse cytogenetics, OS in patients with low *p15* expression was significantly shorter than those with high *p15* expression ($P=0.027$) (Figure 1c). There were also significant differences between the *p15* expression level and DFS ($P=0.029$) or EFS ($P=0.028$) in these patients (data not shown). In this study, the trend toward inferior clinical outcome in patients with FLT3-ITD did not reach statistical significance, possibly due to a small number of patients with FLT3-ITD ($P=0.064$). In addition, D835 mutation of the *FLT3* gene had little influence on the survival, which was in line with the previous reports. When patients without FLT3-ITD were analyzed, high *p15* expression was also associated with significantly longer DFS ($P=0.041$), EFS ($P=0.018$) and OS ($P=0.014$) in patients with intermediate or adverse cytogenetics (Figure 1d and data not shown). A multivariate analysis revealed that low *p15* expression was an independent unfavorable prognostic factor in predicting EFS in all 98 evaluable patients ($P=0.042$), in addition to a trend toward significance in DFS ($P=0.12$) and OS ($P=0.075$). In AML patients with intermediate or adverse cytogenetics, the multivariate analysis showed that low *p15* expression was an independent unfavorable prognostic factor for predicting DFS ($P=0.0050$), EFS ($P=0.015$) and OS ($P=0.014$).

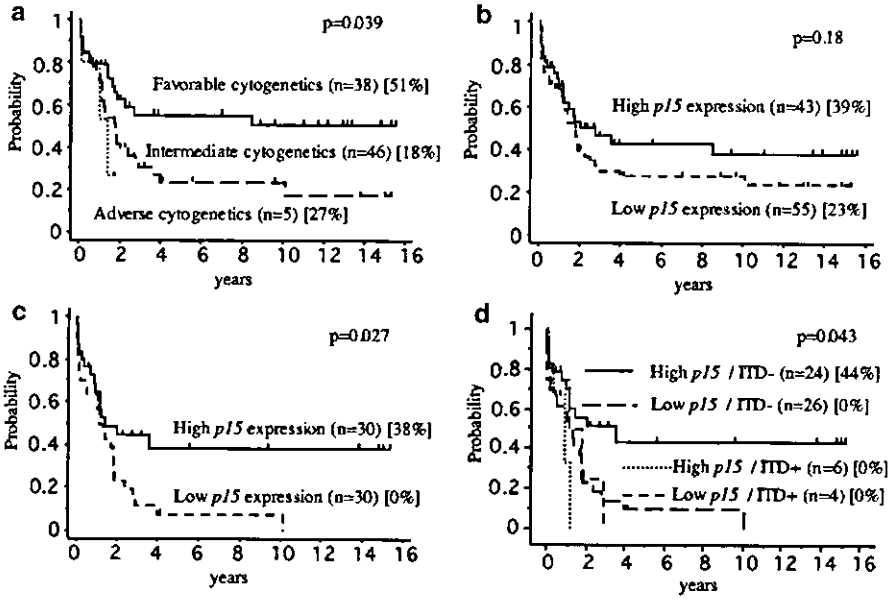

Figure 1 OS in AML patients according to the *p15* expression level: (a) OS in 89 evaluable patients who were treated with intensive chemotherapy according to the cytogenetic risk group; (b) OS in 98 evaluable patients according to the *p15* expression level; (c) OS in 60 patients with intermediate or adverse cytogenetics according to the *p15* expression level; (d) OS in patients with intermediate or adverse cytogenetics according to the *p15* expression level and the presence or absence of the FLT3-ITD. Statistical differences were evaluated by the log-rank test.

In the present study, no significant difference was found in survival according to the *p15* expression level among all evaluable AML patients. Although we found no difference in survival according to the *p15* expression level in patients with favorable cytogenetics, low *p15* expression significantly correlated to unfavorable clinical outcome among the remaining 60 patients with intermediate or adverse cytogenetics. We previously reported that *p15* inactivation by deletion and methylation was highly associated with poor DFS in adult patients with precursor B-cell acute lymphoblastic leukemia.[7] Inactivation of the *p15* gene would increase the risk of relapse by escaping the effect of TGF-β-mediated growth suppression, resulting in progression of cell growth and inhibition of apoptosis.[8] However, *p15* inactivation is not thought to be a very powerful regulator of cell proliferation, and thus it may not influence the clinical outcome in patients with favorable cytogenetics who show a good response to treatment. On the other hand, patients with intermediate or adverse cytogenetics who show a poor response to treatment might be susceptible to the proliferative effect caused by *p15* silencing. Our results suggest that low *p15* expression detected by RQ-PCR could be a useful marker for prognosis in AML patients, especially in the intermediate or adverse cytogenetic risk group. The demethylating agent 5-Aza-dC has been shown to reverse the hypermethylation of the *p15* gene *in vitro* and *in vivo*. We also showed 2–5-fold increases in *p15* mRNA expression after 5-Aza-dC treatment in four of seven fresh leukemic cells from AML patients *in vitro*. This suggests that patients with low p15 expression may benefit from treatment with demethylating agents.

Acknowledgements

We greatly appreciate Drs H Suzushima and F Kawano for their kind help. We are also very grateful to Ms M Ichinomiya for technical assistances. This work was supported in part by Grants-in-Aid for Scientific Research from the Japanese Ministry of Education, Science and Culture, and Grants-in-Aid for Cancer Research from the Japanese Ministry of Health and Welfare.

N Matsuno[1]
K Hoshino[1]
T Nanri[1]
T Kawakita[1]
H Mitsuya[1]
N Asou[1]

[1]*Department of Internal Medicine II, Kumamoto University School of Medicine, Kumamoto, Japan,*

References

1 Herman JG, Civin CI, Issa JP, Collector MI, Sharkis SJ, Baylin SB. Distinct patterns of inactivation of p15INK4B and p16INK4A characterize the major types of hematological malignancies. *Cancer Res* 1997; **57**: 837–841.
2 Aggerholm A, Guldberg P, Hokland M, Hokland P. Extensive intra- and interindividual heterogeneity of p15INK4B methylation in acute myeloid leukemia. *Cancer Res* 1999; **59**: 436–441.
3 Wong IH, Ng MH, Huang DP, Lee JC. Aberrant p15 promoter methylation in adult and childhood acute leukemias of nearly all morphologic subtypes: potential prognostic implications. *Blood* 2000; **95**: 1942–1949.
4 Teofili L, Martini M, Luongo M, Diverio D, Capelli G, Breccia M *et al.* Hypermethylation of GpG islands in the promoter region of p15(INK4b) in acute promyelocytic leukemia represses p15(INK4b) expression and correlates with poor prognosis. *Leukemia* 2003; **17**: 919–924.
5 Cameron EE, Baylin SB, Herman JG. p15(INK4B) CpG island methylation in primary acute leukemia is heterogeneous and suggests density as a critical factor for transcriptional silencing. *Blood* 1999; **94**: 2445–2451.
6 Matsuno N, Osato M, Yamashita N, Yanagida M, Nanri T, Fukushima T *et al.* Dual mutations in the AML1 and FLT3 genes are associated with leukemogenesis in acute myeloblastic leukemia of the M0 subtype. *Leukemia* 2003; **17**: 2492–2499.
7 Hoshino K, Asou N, Okubo T, Suzushima H, Kiyokawa T, Kawano F *et al.* The absence of the p15INK4B gene alterations in adult patients with precursor B-cell acute lymphoblastic leukaemia is a favourable prognostic factor. *Br J Haematol* 2002; **117**: 531–540.
8 Hannon GJ, Beach D. p15INK4B is a potential effector of TGF-beta-induced cell cycle arrest. *Nature* 1994; **371**: 257–261.

A 4′-*C*-Ethynyl-2′,3′-Dideoxynucleoside Analogue Highlights the Role of the 3′-OH in Anti-HIV Active 4′-*C*-Ethynyl-2′-deoxy Nucleosides

Maqbool A. Siddiqui,[†] Stephen H. Hughes,[‡] Paul L. Boyer,[‡] Hiroaki Mitsuya,[§] Que N. Van,[∥] Clifford George,[⊥] Stefan G. Sarafinanos,[○] and Victor E. Marquez*,[†]

Laboratory of Medicinal Chemistry, Center for Cancer Research, NCI-Frederick, NIH, Frederick, Maryland 21702, HIV Drug Resistance Program, Center for Cancer Research, NCI-Frederick, NIH, Frederick, Maryland 21702, Experimental Retrovirology Section, Center for Cancer Research, NCI, NIH, Bethesda, Maryland 20892, NMR Group, Laboratory of Proteomics and Analytical Technologies, SAIC Frederick, Frederick, Maryland 21702, Laboratory for the Structure of Matter, Naval Research Laboratory, Washington, D.C. 20375, and Center for Advanced Biotechnology and Medicine and Chemistry Department, Rutgers University, Piscataway, New Jersey 08854

Received June 8, 2004

4′-*C*-Ethynyl-2′-deoxynucleosides belong to a novel class of nucleoside analogues endowed with potent activity against a wide spectrum of HIV viruses, including a variety of resistant clones. Although favorable selectivity indices were reported for several of these analogues, some concern still exists regarding the 3′-OH group and its role in cellular toxicity. To address this problem, we removed the 3′-OH group from 4′-*C*-ethynyl-2′-deoxycytidine (**1a**). This compound was chosen because of its combined high potency and low selectivity index. The removal of the 3′-OH was not straightforward; it required a different synthetic approach from the one used to synthesize the parent compound. Starting with glycidyl-4-methoxyphenyl ether, the target 4′-*C*-ethynyl-2′,3′-dideoxycytidine analogue (***rac*-1h**) was obtained after 13 steps. In a cellular assay, ***rac*-1h** was completely inactive (0.001−10 μM) against HIV_{LAI}, demonstrating the critical importance of the 3′-OH for antiviral activity. To determine whether the role of the 3′-OH was essential for the phosphorylation of the compound by cellular kinases or for inhibition of DNA polymerization, we synthesized and tested the 5′-triphosphate (***rac*-1h-TP**) for its ability to inhibit HIV reverse transcriptase (RT). ***rac*-1h-TP** was slightly more potent than AZT-5′-triphosphate against wild-type HIV RT, suggesting that the role of the 3′-OH is crucial only for the activation of the drug by cellular kinases. The lipase-catalyzed resolution of ***rac*-1h** into ***ent*-1h** (β-D-dideoxyribo) and ***ent*-14** (β-L-dideoxyribo) and the synthesis of the corresponding 5′-triphosphates established the stereochemical assignment based on HIV RT's preference for the β-D-enantiomer, which was confirmed by assaying against the M184V variant, an RT mutant with a marked preference for incorporating nucleosides in the D-configuration.

Introduction

4′-*C*-Ethynyl-2′-deoxy-β-D-nucleosides (**1a−e**) have been identified as some of the most potent analogues against HIV-1, including several multidrug-resistant strains and HIV-2.[1,2] Although no studies with the corresponding 5′-triphosphates have been performed to elucidate the exact mechanism of antiretroviral activity, the antiviral profile fits that of an NRTI with a mechanism of action similar to that of AZT. This means that 4′-*C*-ethynyl nucleosides suppress HIV replication at or around the step of reverse transcription. Indeed, the fact that the anti-HIV activity of the cytidine (**1a**) and guanosine (**1e**) analogues was reversed by the addition of their physiologic 2′-deoxynucleoside counterparts provides strong evidence that 4′-*C*-ethynyl-2′-deoxy-β-D-nucleosides serve as substrates for HIV RT.[2]

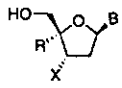

1a	R = C≡CH	X = OH	B = cytosine
1b	R = C≡CH	X = OH	B = 5-F-cytosine
1c	R = C≡CH	X = OH	B = adenine
1d	R = C≡CH	X = OH	B = 2,6-diaminopurine
1e	R = C≡CH	X = OH	B = guanine
1f	R = N_3	X = OH	B = thymine
1g	R = CN	X = OH	B = thymine
1h	R = C≡CH	X = H	B = cytosine

Previous reports of other 4′-substituted-2′-deoxy-β-D-nucleosides, such as 4′-azidothymidine (**1f**), have shown that following intracellular anabolism to the 5′-triphosphate, HIV reverse transcriptase (RT) efficiently incorporated the nucleotide, which prevented further chain elongation of the viral DNA.[3,4] Because these compounds bear no structural resemblance to traditional chain terminators, all of which lack the 3′-OH group, they must have a different mechanism of action. In the case of 4′-azidothymidine (**1f**), the rate of incorporation of the 5′-triphosphate by cellular polymerases

* Author to whom correspondence should be addressed. E-mail: marquezv@dc37a.ncl.nih.gov.
† Laboratory of Medicinal Chemistry, NCI-Frederick.
‡ HIV Drug Resistance Program, NCI-Frederick.
§ Experimental Retrovirology Section, NCI, NIH.
∥ NMR Group, Laboratory of Proteomics and Analytical Technologies, SAIC Frederick.
⊥ Laboratory for the Structure of Matter, Naval Research Laboratory.
○ Rutgers University.

10.1021/jm049550o CCC: $27.50
Published on Web 09/01/2004

was found to be dramatically different when compared to that of HIV RT. Although the rate of incorporation for the former was quite low, HIV RT was able to incorporate two consecutive molecules efficiently. The subsequent distortion of the growing primer brought about by this incorporation seems to prevent further DNA chain elongation, thus causing a delayed chain termination.[3,4] Other structurally similar compounds probably have comparable mechanisms of action, for example, 4′-cyanothymidine (**1g**) and the corresponding cytidine and uridine analogues, all of which are potent inhibitors of HIV replication in cell culture.[5] As a group, 4′-substituted-2′-deoxy-β-D-nucleosides are quite attractive because of the intriguing connection between their novel mechanism of action and their potent activity against multidrug-resistant (MDR) HIV-1 strains. Their efficacy against MDR strains may depend on two important factors: (1) delayed chain termination occurring beyond the polymerase active site and (2) difficulties in selecting mutants that discriminate against the incorporation of analogues that still retain the natural 3′-OH.[2]

Extensive studies with other 4′-substituted-2′-deoxy-β-D-nucleosides with a thymine nucleobase and a variety of substituents, including ethyl, hydroxyethyl, and ethenyl, at the 4′-position demonstrated the superior potency of the ethynyl group.[6] Similarly, for compounds with a cytosine nucleobase, the ethynyl group as in **1a** was the most potent analogue although some host cellular toxicity was encountered.[7] Surprisingly, the 5-fluorocytosine analogue (**1b**) was less toxic and quite potent. Other important structural changes including the use of purine nucleobases, such as adenine (**1c**) and 2,6-diaminopurine (**1d**), produced compounds active against MDR HIV-1 that were less toxic than their counterparts with pyrimidine nucleobases.[1]

Because the 3′-OH in all of these 4′-substituted nucleosides could function as a key element for substrate recognition by cellular kinases and/or polymerases, we decided to investigate the importance of the 3′-OH by deleting it from the most attractive series of 4′-substituted nucleosides, the 4′-*C*-ethynyl-2′-deoxy-β-D-nucleosides. Previous studies have shown that removal of the 3′-OH from the 4′-azido (**1f**) and 4′-cyano (**1g**) analogues resulted either in a complete loss of activity or a significant reduction in potency.[5,8] However, with the structurally related 3′,4′-fused oxetane derivative with a thymine nucleobase, there was only a moderate drop in potency, suggesting that the ether oxygen could have partially fulfilled the role of the 3′-OH.[9] Despite the expected loss of activity similar to what was seen with the 4′-azido analogue (**1f**), removing the 3′-OH from 4′-*C*-ethynyl-2′-deoxy-β-D-nucleosides to generate a 4′-*C*-ethynyl-2′,3′-dideoxy-β-D-nucleoside, such as **1h**, provided the opportunity to assess the role of the 3′-OH during activation and polymerization and in generating cellular toxicity. Because the issue of toxicity was very important, cytosine analogue **1h** was selected to be the target because its progenitor **1a** combined potent activity with significant cellular toxicity.

Chemistry

The required 4-branched-2,3-dideoxysugar **2** was prepared according to a previously published method

Scheme 1[a]

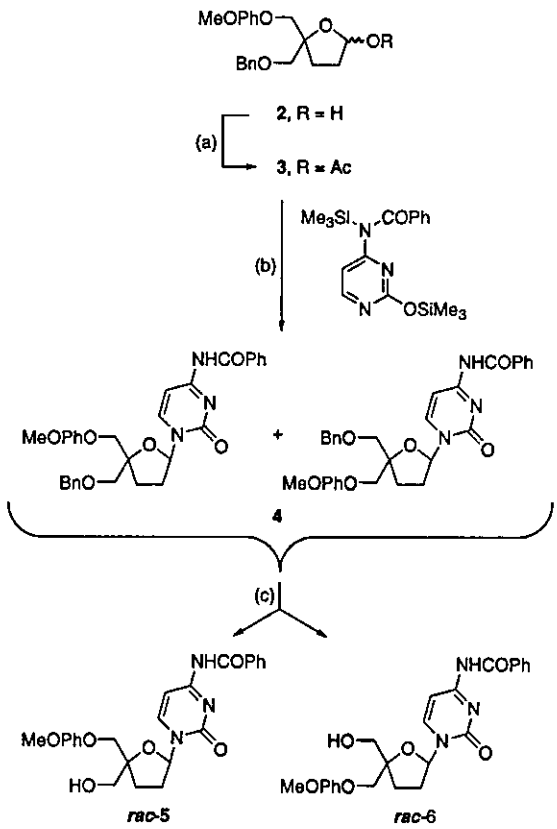

[a] (a) $(CH_3CO)_2O$/pyridine (86%); (b) TMSOTf, CH_2Cl_2 (100%); (c) BCl_3, CH_2Cl_2, −78 °C (*rac*-**6**, 49%; *rac*-**5**, 25%).

in which compound **2** was generated only as an intermediate and not fully characterized.[10] The procedure was repeated, and compound **2** was completely characterized. Acylation of the free hydroxyl group to give **3** followed by standard nucleoside synthesis with persilylated N^4-benzoylcytosine proceeded uneventfully to afford an inseparable mixture of two diastereoisomers (**4**, Scheme 1). The removal of the benzyl protecting group gave a separable mixture of *rac*-**5** and *rac*-**6**, which differ in terms of their relative stereochemistry. Because the correct stereochemical assignment was not clarified until the target compounds were reached (vide infra), the same chemical steps were performed separately on *rac*-**5** and *rac*-**6** but are shown only for one diastereoisomer (*rac*-**5**, Scheme 2).

The oxidation of the hydroxymethyl group to a formyl group (*rac*-**7**) was followed by Wittig olefination with (chloromethyl)triphenylphosphonium chloride to afford chlorovinyl derivative *rac*-**8**. Without isolation, the chlorovinyl group was converted to the ethynyl group after treatment with *n*-butyllithium in tetrahydrofuran to give *rac*-**9**. Finally, deprotection of the *p*-methoxyphenyl group with ammonium cerium (IV) nitrate provided the desired target *rac*-**1h**. Following an identical approach from *rac*-**6** produced *rac*-**10**. At this stage, NMR nOe buildup data adequately determined the relative stereochemistry. In *rac*-**10**, the nOe build ups indicated a distance between H-5′a,b and H-1′ (nucleoside numbering) of 3.3 Å, whereas no nOe was observed between the same set of protons in *rac*-**1h**. Buildup

Scheme 2[a]

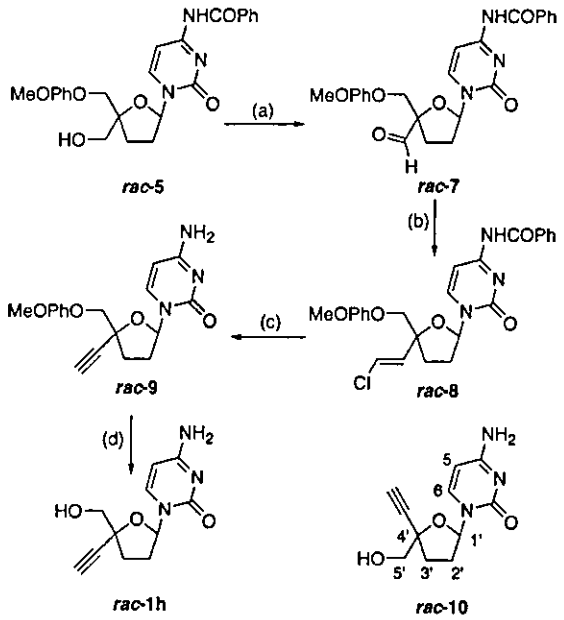

[a] (a) DCC, DMSO, 0 °C (93%); (b) $ClCH_2P(C_6H_5)_3Cl$, *n*-BuLi, THF, −78 °C; (c) *n*-BuLi, THF, −78 °C (48.5% two steps); (d) $(NH_4)_2Ce(NO_3)_6$, CH_3CN:H_2O, 0 °C (83%).

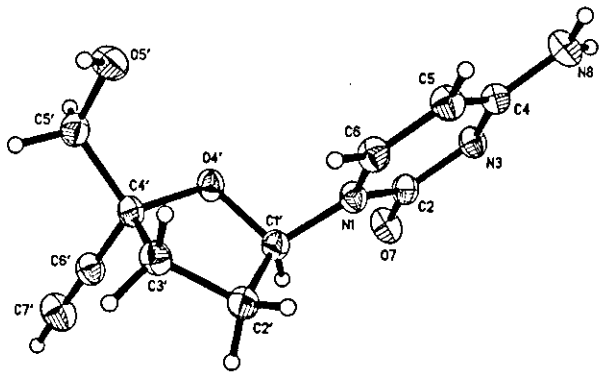

Figure 1. Displacement elliposoid plot of ***rac*-1h** drawn at the 30% probability level.

curves were obtained by irradiating the key target protons on both samples and using an internuclear distance of 2.4 Å between H-6 and H-5 (nucleoside numbering) as a reference for the calculations. During the NMR experiments, it was noticed that ***rac*-1h** crystallized readily and provided suitable crystals for X-ray analysis. As shown in Figure 1, the crystal structure of ***rac*-1h** corresponded to the desired (2*R*,5*R* or 2*S*,5*S*)-(±)-1-(2′,3′-dideoxy-4′-*C*-ethynyl-ribopentofuranosyl)cytosine.

At this point, a lipase-catalyzed approach was used to resolve ***rac*-1h**. To avoid complications with possible interference by the exocyclic amino group during trans esterification with vinyl acetate, which included acetylation or formation of a Schiff base with the released acetaldehyde, this group was protected as a benzoyl amide using the well-known transient protection method to give ***rac*-11** (Scheme 3).[11] Following a 10-day incubation of ***rac*-11** with lipase PS-C "Amano" and vinyl

Scheme 3[a]

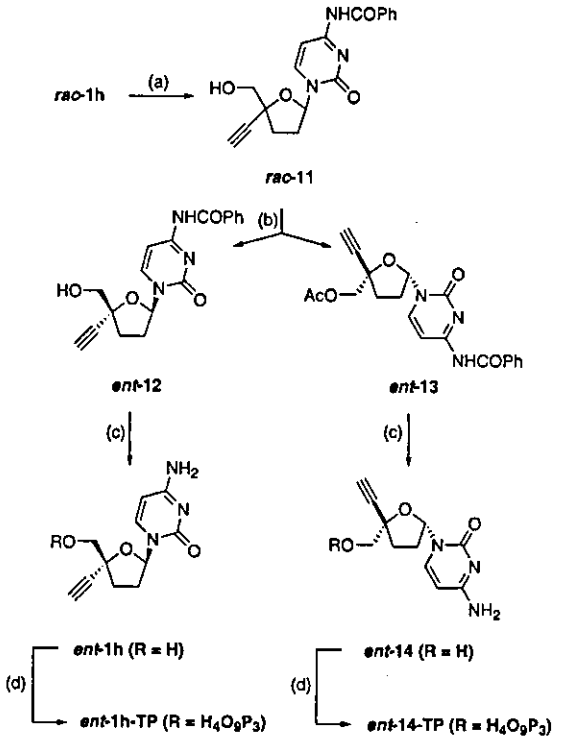

[a] (a) i. TMSCl, pyridine, ii. PhCOCl, iii. NH_4OH (66.5%); (b) lipase PS−C Amano I, CH_2=CHOAc, CCl_4/$CHCl_3$ (***ent*-13**, 58%; ***ent*-12**, 40.5%) (c) satd NH_3/CH_3OH (70%); (d) performed by TriLink Biotechnologies, Inc., San Diego, CA (www.trilinkbiotech.com).

acetate, the less polar monoacetate (***ent*-13**) was obtained as a single enantiomer (91% ee) after flash column chromatography. The mixture of unreactive alcohols was then treated for a second time with the enzyme under the same conditions to give, after column chromatography, enantiomerically pure ***ent*-12** (98% ee). The removal of the N^4-benzoyl group from ***ent*-12** and the acetyl/N^4-benzoyl groups from ***ent*-13** gave the desired β-D-dideoxyribo targets: ***ent*-1h** and β-L-dideoxyribo enantiomer ***ent*-14**. This assignment was based on the capacity of HIV-1 RT to discriminate between the enantiomers (vide infra) and, more recently, on the synthesis of the authentic β-D-dideoxyribo enantiomer (***ent*-1h**) obtained from a chiral lactone precursor to **2**[12] using a method similar to that shown in Schemes 1 and 2. The synthesis of the corresponding 5′-triphosphates, ***ent*-1h-TP** (β-D-dideoxyribo) and ***ent*-14-TP** (β-L-dideoxyribo), was performed by conventional methods. The 5′-triphosphate of the racemate, ***rac*-1h-TP**, was also synthesized as a reference.

Biological Activity

Relative to 4′-*C*-ethynyl-2′-deoxycytidine (**1a**), dideoxy analogue ***rac*-1h** was inactive in vitro against HIV_{LAI} when tested in a concentration range between 0.001 and 10 μM in MT-2 and MT-4 cells. Under the same experimental conditions, control AZT had an IC_{50} of 0.014 μM. These results underscore the critical role of the 3′-OH group for anti-HIV activity in a cellular system. To determine whether the role of the 3′-OH was crucial for the activation step(s) or for the inhibition of

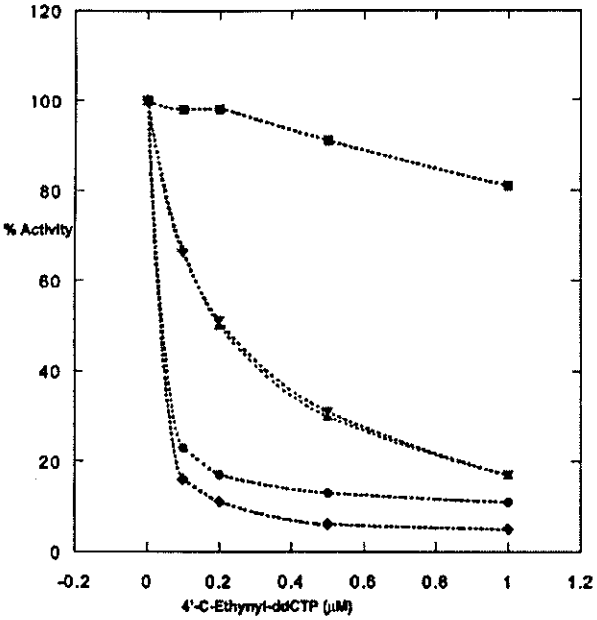

Figure 2. Inhibition of HIV RT wild type and M184V mutant strains by racemic (***rac*-1hTP**) and enantiomeric (***ent*-1hTP** and ***ent*-14TP**) 5′-triphosphates of 1-(2′,3′-dideoxy-4-*C*-ethynyl-ribofuranosyl)cytosine: ***rac*-1h-TP** (wild type = ●); ***ent*-1h-TP** (wild type = ◆); ***ent*-1h-TP** (M184V = ▼); ***ent*-14-TP** (wild type = ▲); ***ent*-14-TP** (M184V = ■).

HIV-1 viral DNA polymerization, we synthesized and tested the 5′-triphosphate (***rac*-1h-TP**) for its ability to inhibit HIV RT. Against wild-type HIV-1 RT, using a single-stranded M13mp18 DNA template and a −47 sequencing primer, ***rac*-1h-TP** was slightly more potent than AZT-5′-triphosphate (not shown), suggesting that the 3′-OH plays a critical role in the activation of the drug by cellular kinases (Figure 2, ●). We expected the enzyme to discriminate between enantiomers ***ent*-1h-TP** (β-D-dideoxyribo) and ***ent*-14-TP** (β-L-dideoxyribo) on the basis of calculations from the molecular docking of the 5′-triphosphates into the active site of HIV RT (vide infra), which predicted that the β-D-dideoxyribo enantiomer (***ent*-1h-TP**) would be the more active isomer. Indeed, the enantiomer presumed to be the β-D-dideoxyribo enantiomer (***ent*-1h-TP**) was more potent in blocking DNA synthesis by wild-type HIV-1 RT than its antipode ***ent*-14-TP** (Figure 2, ◆ versus ▲). The fact that the M184V mutant of HIV-1 RT has a greater selectivity against β-L-nucleosides than does wild type[13-16] also confirmed the assignment of D- and D-enantiomers: the β-L-dideoxyribo enantiomer (***ent*-14-TP**) was virtually inactive (Figure 2, ■), whereas the β-D-dideoxyribo enantiomer (***ent*-1h-TP**) strongly inhibited the M184 mutant RT despite a low level of resistance (Figure 2, ▼). This low level of resistance of M184V for the β-D-dideoxyribo (***ent*-1h-TP**) enantiomer is not surprising because M184V has been reported to show a low level of resistance to ddCTP.[17,18]

In light of a recent investigation reporting that the L-enantiomer of **1a** is inactive against the HIV virus in cell culture, [19] it is interesting that ***ent*-14-TP** is active against wild-type HIV-1 RT. In fact, the level of potency of ***ent*-14-TP** against wild-type HIV-1 RT is identical to that of ***ent*-1h-TP** against the M184V mutant (Figure 2, ▲ versus ▼). On the basis of these results, it would appear that the 3′-OH of the β-D enantiomer of **1a** is critical for phosphorylation by cellular kinases, but in the L-enantiomer, it must play a negative role by occupying an unfavorable position in the active site of the kinase. The removal of the 3′-OH from either enantiomer produces inactive compounds in cell-based assays, but to a varying degree, both 5′-triphosphates seem to be acceptable substrates for HIV-1 RT. According to a recent report, the combined removal of the 3′-OH and the flattening of the dideoxyribose ring by a 2′,3′ double bond restores anti-HIV activity in MT-2 cells.[20] This finding seems to be consistent with our own observations correlating a reduced puckering amplitude with substrate recognition by both cellular kinases and polymerases.[21]

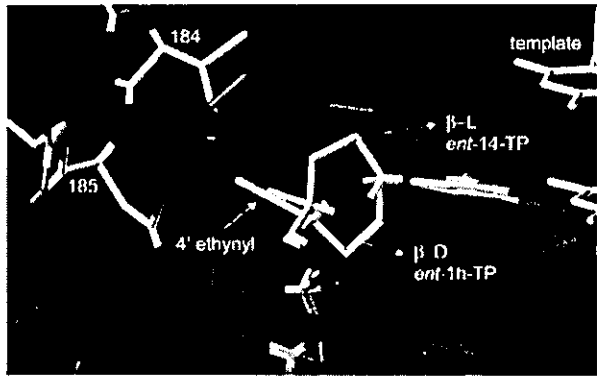

Figure 3. Superposition of ***ent*-1h-TP** and ***ent*-14-TP** at the active site of HIV RT showing a measurable deviation of the 4′-ethynyl moiety.

Crystal Structure and Docking of 5′-Triphosphates at the Active Site of HIV RT

On the basis of the torsion angles obtained from the crystal structure (Figure 1), the dideoxyribose moiety of ***rac*-1h** has a *P* value of 43.49° in the pseudorotational cycle, almost exactly in the middle of a $^3T_4$ ($P = 36°$) and 4′-*exo* ($_4E$, $P = 54°$) conformations. This is clearly in the Northern Hemisphere but slightly beyond the range that is observed for most conventional nucleosides (0−36°). The molecule also has a highly puckered ring with a ν_{max} of 37.10°. The X-ray coordinates of ***rac*-1h** were used to construct the 5′-triphosphates of ***ent*-1h-TP** and ***ent*-14-TP** for computer docking studies with HIV RT. When the two structures are superposed at the polymerase site of an HIV RT/DNA/nucleotide ternary complex, there is a measurable deviation in the direction of the 4′-ethynyl moiety between the two enantiomers (Figure 3). The D enantiomer (***ent*-1h-TP**) appears to fit nicely at the active site of wild-type HIV RT (Figure 4A), and consistent with the low level of resistance observed against the M184V mutant (Figure 2, ▼), the docking in Figure 4C shows some negative steric interaction with Val184. The situation with the L enantiomer (***ent*-14-TP**) would indicate that relative to ***ent*-1h-TP** the fit with respect to Met184 is somewhat tighter (Figure 4B), plus there could be some steric interactions in wild-type HIV RT with Tyr115 and/or Ala114, or with both (Figure 5). It is possible that the steric interactions of the L enantiomer with these amino acids could be alleviated either by a torsional rotation

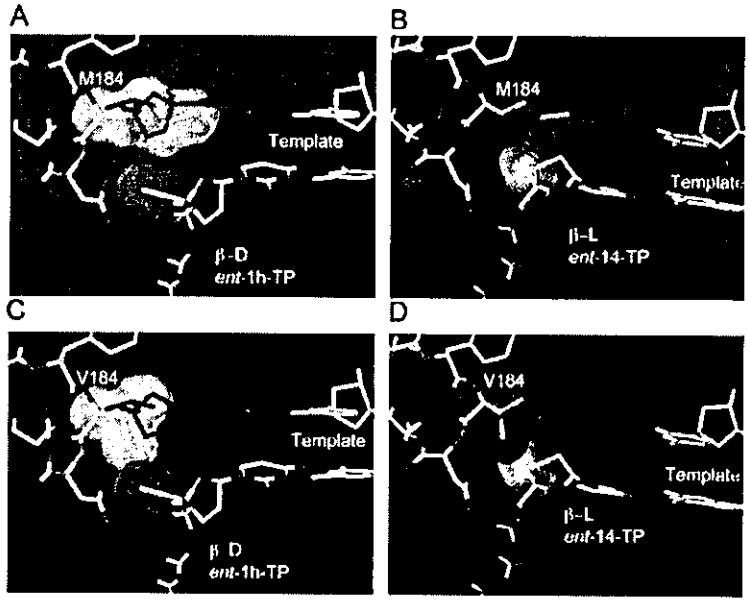

Figure 4. (A) β-D-enantiomer (***ent*-1h-TP**) at the active site of wild-type HIV RT. Volumes for the 4'-ethynyl group (green) and methionine184 (yellow). (B) β-L-enantiomer (***ent*-14-TP**) at the active site of wild-type HIV RT. Volumes for the 4'-ethynyl group (yellow) and methionine184 (green). (C) β-D-enantiomer (***ent*-1h-TP**) at the active site of M184V HIV RT. Volumes for the 4'-ethynyl group (green) and methionine184 (yellow). (D) β-L-enantiomer (***ent*-14-TP**) at the active site of M184V HIV RT. Volumes for the 4'-ethynyl group (yellow), methionine184 (green), and steric clash (orange).

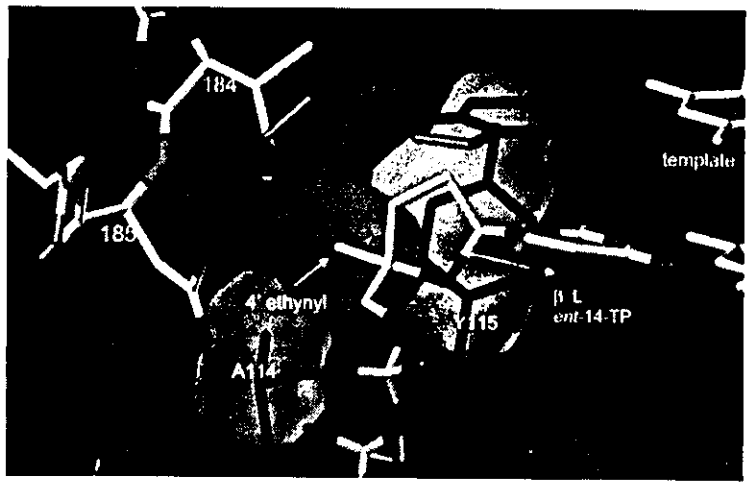

Figure 5. β-L-enantiomer (***ent*-14-TP**) at the active site of wild-type HIV RT. Volumes for the 4'-ethynyl group (green), alanine and tyrosine (yellow), and steric clash (orange).

of Tyr115 or a small rearrangement of the L nucleotide, explaining the lower level of potency observed for this enantiomer against wild-type HIV-1 RT (Figure 2, ▲). However, it is clear that for the M184V mutant the steric clash between the Cγ of the β-branched valine with the 4'-ethynyl group of ***ent*-14-TP** (Figure 4D) and possibly with the L-dideoxy ring (not shown) would prevent the L enantiomer from binding to the active site in a productive manner, explaining its lack of activity (Figure 2, ■).

Discussion

The inactivity of 1-(2',3'-dideoxy-4'-*C*-ethynyl-ribopentofuranosyl)cytosine (***rac*-1h**) as an inhibitor of HIV replication in cultured cells highlights the importance of the 3'-OH as a key determinant for activity for the 4'-*C*-ethynyl-2'-deoxy-β-D-nucleosides and, by extension, for other 4'-substituted 2'-deoxynucleosides that are active against HIV (vide supra). The potent inhibition of HIV-1 RT by the 5'-triphosphate (***rac*-1h-TP**) confirms that the failure of this agent to exert good anti-HIV activity in the cell culture results from the failure of the cellular kinases to generate the requisite 5'-triphosphate. In the present work, the racemate 1-(2',3'-dideoxy-4'-*C*-ethynyl-ribopentofuranosyl)cytosine (***rac*-1h**) was resolved into its components, β-D-dideoxyribo (***ent*-1h**) and β-L-dideoxyribo (***ent*-14**), by a lipase-catalyzed reaction. The assignment of the absolute stereochemistry was confirmed by HIV RT's preference for the natural β-D-configuration. This assignment was confirmed using the M184V mutant, which has a much greater preference for the D enantiomers. The synthesis of authentic ***ent*-1h** also confirmed this assignment because its 5'-triphosphate showed identical activity as

the β-D-dideoxyribo isomer separated by the lipase-catalyzed resolution (data not shown). The results presented here suggest, on the basis of the strong anti-HIV activity of the 5′-triphosphate, ***ent*-1h-TP**, that the 2′,3′-dideoxy-4′-*C*-ethynyl-β-D-ribopentofuranosyl nucleoside template is an attractive scaffold for the development of prodrugs capable of bypassing the first kinase. These types of compounds may also offer an additional advantage of having reduced toxicity because the lack of 3′-OH prevents them from being good substrates for cellular polymerases.

General Experimental Section

All chemical reagents were commercially available. Column chromatography was performed on silica gel 60, 230−240 mesh (E. Merck), and analytical TLC was performed on Analtech Uniplates silica gel GF. Routine IR and ^{1}H NMR spectra were recorded using standard methods. Positive-ion fast-bombardment mass spectra (FABMS) were obtained on a VG 7070E mass spectrometer at an accelerating voltage of 6 kV and a resolution of 2000. Glycerol was used as the sample matrix, and ionization was effected by a beam of xenon atoms. Elemental analyses were performed by Atlantic Microlab, Inc., Norcross, GA.

5-[(4-Methoxyphenoxy)methyl]-5-(phenylmethoxy)-methyl]oxolan-2-ol (2). This compound was reported in ref 10 but was not full characterized. We followed the same procedure and obtained **2** as an oil (mixture of anomers): ^{1}H NMR ($CDCl_3$) δ 7.30 (m, 5 H, PhH), 6.80 (m, 4 H, ArH), 5.51 (irregular t, 0.5 H, H-2), 5.46 (dd, J = 7.5, 4.2 Hz, 0.5 H, H-2), 4.60 (AB q, J = 11.8 Hz, 1 H, PhCH_2O), 4.52 (AB q, J = 12.3 Hz, 1 H, PhCH_2O), 3.80 (AB q, J = 9.2 Hz, 1 H, BnOCH_2 or ArOCH_2), 3.74 (s, 3 H, OCH_3), 3.64 (AB d, J = 1.0 Hz, 1 H, BnOCH_2 or ArOCH_2), 3.58 (d, J = 7.5 Hz, 0.5 H, BnOCH_2 or ArOCH_2), 3.46 (AB q, J = 9.5 Hz, 1 H, BnOCH_2 or ArOCH_2), 3.12 (d, J = 7.5 Hz, 0.5 H, BnOCH_2 or ArOCH_2), 1.90−2.20 (m, 4 H, H-$3_{a,b}$ and H-$4_{a,b}$); FAB-MS (relative intensity) 344 ($M^{+\cdot}$, 89). Anal. Calcd for $C_{20}H_{24}O_5$: C, 69.75; H, 7.02. Found: C, 69.60; H, 7.06.

5-[(4-Methoxyphenoxy)methyl]-5-[(phenylmethoxy)-methyl]oxolan-2-yl acetate (3). A solution of lactol **2** (6.10 g, 17.7 mmol) in dry pyridine (90 mL) was treated with acetic anhydride (4.2 mL, 44.4 mmol). After stirring at room temperature for 72 h, the reaction mixture was diluted with EtOAc (200 mL), washed with water (3 × 100 mL), dried ($MgSO_4$), and concentrated under vacuum. The crude residue was purified by flash column chromatography on silica gel using EtOAc/hexanes (1:6 → 1:3) to give 5.93 g (86.7%) of **3** as a clear oil (mixture of anomers); ^{1}H NMR ($CDCl_3$) δ 7.25 (m, 5 H, PhH), 6.80 (m, 4 H, ArH), 6.32 (m, 1 H, H-2), 4.50−4.60 (overlapping s and AB q, J = 12.4 Hz, 2 H, PhCH_2O), 3.80−4.00 (2 AB q, J = 9.4 Hz, 2 H, BnOCH_2 or ArOCH_2), 3.73 and 3.74 (s, 3 H, OCH_3), 3.48−3.62 (overlapping s and AB q, J = 9.8 Hz, 2 H, $BnOCH_2$ or $ArOCH_2$), 1.90−2.30 (m, 4 H, H-$3_{a,b}$ and H-$4_{a,b}$), 1.93 and 1.94 (s, 3 H, $OCOCH_3$); FAB-MS (relative intensity) 387 (MH^+, 25), 386 ($M^{+\cdot}$, 100). Anal. Calcd for $C_{22}H_{26}O_6$: C, 68.37; H, 6.78. Found: C, 68.38; H, 6.77.

***N*-(1-{5-[(4-Methoxyphenoxy)methyl]-5-[(phenyl-methoxy)methyl]oxolan-2-yl}-2-oxohydropyrimidin-4-yl)benzamide (4).** N^4-Benzoylcytosine (5.30 g, 24.6 mmol) was suspended in dry CH_3CN (20 mL) and was treated with bis-(trimethylsilyl)trifluoroacetamide (BSTFA, 20 mL, 75.3 mmol) under argon. After 1 h of stirring, the reaction mixture became homogeneous. The volatiles were removed under vacuum to give the silylated base as a thick oil. Separately, a solution of acetate **3** (6.29 g, 16.3 mmol) in dry $ClCH_2CH_2Cl$ (100 mL) was added to the silylated base followed by the slow addition of trimethylsilyl trifluoromethanesulfonate (TMSOTf, 4.8 mL, 26.4 mmol). The reaction mixture was stirred at room temperature for 20 h and was diluted with CH_2Cl_2 (100 mL). After cooling to 0 °C, the reaction was quenched by the addition of a saturated solution of $NaHCO_3$. The suspension that was obtained was filtered, and the organic layer was separated, dried ($MgSO_4$), and concentrated under vacuum. The crude product that was obtained was purified by flash chromatography on silica gel using EtOAc/hexanes (1:1 → pure EtOAc) to give a quantitative yield of a yellowish foam consisting of an inseparable mixture of two diastereoisomers (**4**). This material was carried out as a mixture in the following debenzylation step.

(2*R*,5*R* or 2*S*,5*S*)-*N*-(1-{5-(Hydroxymethyl)-5-[(methoxy-phenoxy)methyl]oxolan-2-yl}-2-oxohydropyrimidin-4-yl)benzamide (*rac*-5) and (2*S*,5*R* or 2*R*,5*S*)-*N*-(1-{5-(Hydroxymethyl)-5-[(methoxyphenoxy)methyl]oxolan-2-yl}-2-oxohydropyrimidin-4-yl)benzamide (*rac*-6). The inseparable mixture of diastereoisomers **4** (4.0 g, 7.38 mmol) was dissolved in anhydrous CH_2Cl_2 (40 mL), cooled to −78 °C, and treated with a solution of BCl_3 in CH_2Cl_2 (1 M, 25 mL). After stirring for 3 h, the reaction was quenched with MeOH (5 mL) and warmed to room temperature. All of the volatiles were removed under vacuum, and the residue was coevaporated three times with MeOH (10 mL). The crude product was purified by flash chromatography on silica gel using EtOAc/hexanes (2:1 → pure EtOAc) to give diastereoisomer ***rac*-5** (0.75 g, 25% yield from **3**) and diastereoisomer ***rac*-6** (1.43 g, 49% yield from **3**) as foams.

Diastereoisomer ***rac*-5**: ^{1}H NMR ($CDCl_3$) δ 8.55 (d, J = 7.6 Hz, 1 H, H-6), 7.50−8.10 (m, 6 H, H-5, PhH), 6.95 (br s, 4 H, ArH), 6.35 (m, 1 H, H-2′), 4.37 (d, J = 10.1 Hz, 1 H, HOCH_2 or ArOCH_2), 4.11 (d, J = 10.1 Hz, 1 H, HOCH_2 or ArOCH_2), 3.90 (s, 3 H, OCH_3), 3.75 (s, 2 H, HOCH_2 or ArOCH_2), 2.85 (m, 1 H, H-3′$_a$ or H-4′$_a$), 2.30 (m, 2 H, H-3′$_{a,b}$ or H-4′$_{a,b}$), 2.10 (m, 1 H, H-3′$_b$ or H-4′$_b$); FAB-MS (relative intensity) 452 (MH^+, 17), 451 ($M^{+\cdot}$, 15), 216 (bH_2^+, 100).

Diastereoisomer ***rac*-6**: ^{1}H NMR ($CDCl_3$) δ 8.38 (d, J = 7.4 Hz, 1 H, H-6), 7.40−7.92 (m, 6 H, H-5, PhH), 6.80 (br s, 4 H, ArH), 6.35 (dd, J = 6.6, 4.3 Hz, 1 H, H-2′), 3.99 (d, J = 11.7 Hz, 1 H, HOCH_2 or ArOCH_2), 3.91 (s, 2 H, HOCH_2 or ArOCH_2), 3.86 (d, J = 11.7 Hz, 1 H, HOCH_2 or ArOCH_2), 3.80 (s, 3 H, OCH_3), 2.80 (m, 1 H, H-3′$_a$ or H-4′$_a$), 2.21 (m, 2 H, H-3′$_{a,b}$ or H-4′$_{a,b}$), 2.15 (m, 1 H, H-3′$_b$ or H-4′$_b$); FAB-MS (relative intensity) 452 (MH^+, 17), 451 ($M^{+\cdot}$, 15), 216 (bH_2^+, 100).

(2*R*,5*R* or 2*S*,5*S*)-6-Amino-3-{5-ethynyl-5-[(4-methoxy-phenoxy)methyl]oxolan-2-yl}-3-hydropyrimidin-2-one (*rac*-9). A solution of ***rac*-5** (0.74 g, 1.63 mmol) and 1,3-dicyclohexylcarbodiimide (DCC, 1.02 g, 4.93 mmol) in anhydrous DMSO (40 mL) was cooled to 0 °C and treated with dichloroacetic acid (0.08 mL, 0.58 mmol). The resulting solution was stirred for 1.5 h while allowing it to reach room temperature. The precipitate formed (dicyclohexylurea, DCU) was filtered off and washed with EtOAc (50 mL), and the combined filtrate was diluted with EtOAc (200 mL) and extracted with water (3 × 100 mL) and brine (2 × 100 mL). The organic layer was separated, dried ($MgSO_4$), and concentrated under vacuum. The residue was purified by flash chromatography on silica gel using EtOAc followed by CH_2Cl_2/MeOH (40:1 → 20:1) to give 0.68 g (93.1%) of aldehyde ***rac*-7**. Thin-layer chromatography on silica gel using $CHCl_3$/*n*-BuOH/acetone (40:25:7.5) revealed some contamination with DCU, and the product was used immediately in the following reaction. A suspension of (chloromethyl)triphenylphosphonium chloride (2.15 g, 6.19 mmol) in anhydrous THF (50 mL) was cooled to −78 °C and treated with a solution of *n*-BuLi in hexanes (1.6 M, 4.0 mL). After 1 h of stirring, a solution of aldehyde ***rac*-7** (0.68 g, 1.51 mmol) in dry THF (50 mL) was added. The temperature of the bath was raised to 0 °C, and stirring continued for 3 h. Following the cautious addition of an aqueous saturated solution of H_4NCl (10 mL), the reaction mixture was extracted with EtOAc (2 × 100 mL). The combined organic layer was washed with brine (2 × 75 mL), dried ($MgSO_4$), and concentrated under vacuum. The crude product (***rac*-8**) was still contaminated with DCU and triphenylphosphine oxide. Hence, it was used as such for the following reaction. Crude ***rac*-8** was dissolved in anhydrous THF (40 mL), cooled to −78 °C, and treated slowly with a solution of *n*-BuLi in hexanes (1.6 M, 20 mL). After stirring

for 2 h, the reaction was quenched by the cautious addition of an aqueous saturated solution of H_4NCl (20 mL). The organic layer was washed with brine (2 × 75 mL), dried ($MgSO_4$), and concentrated under vacuum. The crude product was purified by flash chromatography on silica gel using CH_2Cl_2/MeOH (40:1 → 10:1) to give ***rac*-9** (0.271 g, 48.5% yield from ***rac*-5**) as a yellowish foam; ^1H NMR ($CDCl_3$) δ 8.04 (d, J = 7.8 Hz, 1 H, H-4), 6.80 (m, 4 H, ArH), 6.18 (dd, J = 6.6, 3.1 Hz, H-2'), 6.08 (d, J = 7.8 Hz, 1 H, H-5), 4.37 (d, J = 10.9 Hz, 1 H, ArOCH_2), 4.10 (d, J = 10.9 Hz, 1 H, ArOCH_2), 3.80 (s, 3 H, OCH_3), 2.80 (m, 1 H, 1 H, H-3'$_a$ or H-4'$_a$), 2.60 (s, 1 H, CC*H*), 2.46 (m, 1 H, 1 H, H-3'$_b$ or H-4'$_b$), 1.98 (m, 2 H, H-3'$_{a,b}$ or H-4'$_{a,b}$); FAB-MS (relative intensity) 342 (MH^+, 40), 112 (bH_2^+, 100). Anal. Calcd for $C_{18}H_{19}N_3O_4 \cdot 0.25CH_3OH$: C, 62.73; H, 5.76; N, 12.03. Found: C, 63.05; H, 5.73; N, 11.63.

(2*R*,5*R* or 2*S*,5*S*)-6-Amino-3-[5-ethynyl-5-(hydroxymethyl)oxolan-2-yl]-3-hydropyrimidin-2-one [(±)-1-(2',3'-dideoxy-4-*C*-ethynyl-ribo-pentofuranosyl)cytosine] (*rac*-1h). A stirred solution of ***rac*-9** (0.261 g, 0.76 mmol) in acetonitrile/water (4:1, 24 mL) was cooled to 0 °C and treated with ammonium cerium (IV) nitrate (1.38 g, 2.51 mmol) for 2.5 h. The solvent was removed under vacuum, and the residue was coevaporated with MeOH (3 × 10 mL). The crude product obtained was purified once by flash chromatography on silica gel with CH_2Cl_2/MeOH (10:1 → 3:1) and twice by reverse-phase C-18 column chromatography eluting first with water and then with MeOH/water (15:1 → 5:1). The combined fractions containing the product were evaporated under vacuum and then lyophilized to give 0.148 g (83%) of product ***rac*-1h**. Recrystallization from MeOH/ether provided a crystalline solid, mp 166–167 °C; ^1H NMR (D_2O) δ 7.66 (d, J = 7.61 Hz, 1 H, H-4), 6.80 (dd, J = 7.5, 3.5 Hz, 1 H, H-2'), 5.90 (d, J = 7.5 Hz, 1 H, H-5), 3.70 (AB q, J = 12.3 Hz, 2 H, HOCH_2), 2.88 (s, 1 H, CC*H*), 2.58 (m, 1 H, H-3'$_a$ or H-4'$_a$), 2.05 (m, 3 H, H-3'$_b$ or H-4'$_b$ plus H-3'$_{a,b}$ or H-4'$_{a,b}$); FAB-MS (relative intensity) 236 (MH^+, 35), 112 (bH_2^+, 100); HRMS (FAB) calcd for $C_{11}H_{14}O_3N_3$: 236.1035. Found: 236.1031.

(2*S*,5*R* or 2*R*,5*S*)-6-Amino-3-[5-ethynyl-5-(hydroxymethyl)oxolan-2-yl]-3-hydropyrimidin-2-one [(±)-1-(2',3'-dideoxy-4-*C*-ethynyl-ribo-pentofuranosyl)cytosine] (*rac*-10). This compound was obtained following the same procedure as described for the other diastereoisomer ***rac*-1h**: ^1H NMR (D_2O) δ 7.86 (d, J = 8.0 Hz, 1 H, H-4), 6.04 (m, 1 H, H-2'), 5.96 (d, J = 7.4 Hz, 1 H, H-5), 3.57 (AB q, J = 11.7 Hz, 2 H, HOCH_2), 3.00 (s, 1 H, CC*H*), 2.45 (m, 1 H, H-3'$_a$ or H-4'$_a$), 2.14 (m, 3 H, H-3'$_b$ or H-4'$_b$ plus H-3'$_{a,b}$ or H-4'$_{a,b}$); FAB-MS (relative intensity) 236 (MH^+, 73), 112 (bH_2^+, 100); HRMS (FAB) calcd for $C_{11}H_{14}O_3N_3$: 236.1035. Found: 236.1034.

(2*R*,5*R* or 2*S*,5*S*)-*N*-{1-[5-Ethynyl)-5-(hydroxymethyl)-oxolan-2-yl]-2-oxohydropyrimidin-4-yl}benzamide (*rac*-11). A solution of ***rac*-1h** (0.085 g, 0.361 mmol) in anhydrous pyridine (15 mL) was treated with chlorotrimethylsilane (TMSCl, 0.35 mL, 2.57 mmol) and stirred at room temperature for 20 min. Benzoyl chloride (0.23 mL, 1.93 mmol) was added, and after 2 h, the reaction was cooled to 0 °C and quenched with water (2 mL). After stirring for 15 min, concentrated NH_4-OH (5 mL) was added, the ice bath was removed, and the solution was left at room temperature for 1 h. All volatiles were removed under vacuum, and the residue was coevaporated three times with MeOH (10 mL). The final residue was purified first by flash column chromatography on silica gel (EtOAc/hexanes, 2:1 → EtOAc) followed by a second purification through a C-18 reversed-phase column (water and water/MeOH, 6:1 → 1:4) to give 0.084 g (68.5%) of ***rac*-11** as a foam; ^1H NMR ($CDCl_3$) δ 8.25 (d, J = 7.4 Hz, 1 H, H-6), 7.82 (d, J = 7.6 Hz, 1 H, H-5), 7.40–7.60 (m, 5 H, PhH), 6.14 (dd, J = 7.0, 3.2 Hz, 1 H, H-2'), 4.01 (d, J = 11.8 Hz, 1 H, CH_2OH), 3.80 (d, J = 11.8 Hz, 1 H, CH_2OH), 2.78 (m, 1 H, H-3'$_a$ or H-4'$_a$), 2.50 (s, 1 H, CC*H*), 2.30 (m, 1 H, H-3'$_b$ or H-4'$_b$), 2.20 (m, 1 H, H-4'$_a$ or H-3'$_a$), 2.80 (m, 1 H, H-4'$_b$ or H-3'$_b$).

Lipase-Catalyzed Resolution. A solution of ***rac*-11** (0.065 g, 0.191 mmol) in $CCl_4/CHCl_3$ (1:1, 20 mL) was treated with vinyl acetate (1 mL, 10.84 mmol) and lipase PS-C Amano I (0.190 g). The mixture was stirred at room temperature for 10 days. The enzyme was removed by filtration through a pad of Celite, and the solid cake was washed with the same solvent mixture of CCl_4 and $CHCl_3$. The combined filtrate was concentrated under reduced pressure, and the residue was purified by flash column chromatography on silica gel ($CHCl_3$/MeOH, 40:1 → 20:1) to give 0.043 g (58%) of the less polar monoacetate, ***ent*-13** (91% ee, chiral HPLC, RT = 22.38 min), and a mixture of the more polar unreactive alcohols. The mixture of unreactive alcohols was treated a second time under the same conditions in $CCl_4/CHCl_3$ (1:1, 10 mL) with the enzyme (0.10 g) and vinyl acetate (1 mL, 10.84 mmol). After flash column chromatography on silica gel under the same chromatographic conditions, 0.030 g of ***ent*-12** (98% ee, chiral HPLC, RT = 14.32 min) was obtained.

***ent*-13. (2*S*,5*S*)-*N*-{1-[5-Ethynyl)-5-(acetoxymethyl)oxolan-2-yl]-2-oxohydropyrimidin-4-yl}benzamide.** ^1H NMR ($CDCl_3$) δ 8.10 (d, J = 7.2 Hz, 1 H, H-6), 7.40–7.84 (m, 6 H, H-5, Ph), 6.16 (dd, J = 6.8, 2.6 Hz, 1 H, H-2'), 4.46 (d, J = 12.1 Hz, 1 H, CH_2OH), 4.34 (d, J = 12.1 Hz, 1 H, CH_2OH), 2.84 (m, 1 H, H-3'$_a$ or H-3'$_b$), 2.54 (s, 1 H, CC*H*), 2.00–2.20 (m, 3 H, H-3'$_a$ or H-3'$_b$ and H-4'$_{a,b}$), 2.10 (s, 3 H, CH_3CO).

***ent*-12: (2*R*,5*R*)-*N*-{1-[5-Ethynyl)-5-(hydroxymethyl)-oxolan-2-yl]-2-oxohydropyrimidin-4-yl}benzamide.** The ^1H NMR of this compound was identical to that of ***rac*-11**.

General Procedure for the Deacylation of *ent*-12 and *ent*-13. The compounds were suspended in a saturated methanolic ammonia solution and kept at room temperature in a sealed tube for 5 days. The solution was concentrated under vacuum, and the solid obtained was purified first by flash column chromatography on silica gel (CH_2Cl_2/MeOH, 10:1 → 6:1) to give a 70% yield of the final deblocked materials (***ent*-1h** and ***ent*-14**) as white foams. Both ^1H NMR spectra were identical to that of ***rac*-1h**. ***ent*-1h**: [a]23D + 45.84 (c 0.59, H_2O). Anal. Calcd for $C_{11}H_{13}N_3O_3 \cdot 0.33\ H_2O$: C, 54.76; H, 5.70; N, 17.41. Found: C, 54.52; H, 5.60; N, 17.33.

Chiral HPLC Chromatography. Chiralcel OD column with hexanes/isopropyl alcohol (1:1) as the eluant; injection volume 10 μL); flow rate 3.0 mL/min; UV detection at 220 nm.

Syntheses of 5'-Triphosphates of *rac*-1h, *ent*-1h, and *ent*-14. The custom syntheses of these 5'-triphosphates were performed by TriLink Biotechnologies, Inc. using conventional methodology. ***rac*-1h-TP** was 95.4% pure by HPLC and >95% pure by ^{31}P NMR; ***ent*-1h-TP** was 97.7% pure by HPLC and >95% pure by ^{31}P NMR; ***ent*-14-TP** was 97.08% pure by HPLC and > 5% by ^{31}P NMR. Additional information is provided as Supporting Information.

nOe Experiments. nOe buildups were not quantitative because the samples were not degassed, but the qualitative buildup data was adequate to determine the relative stereochemistry. In ***rac*-10**, the nOe data gave a distance between H-5'a,b and H-1' (nucleoside numbering) of 3.3 Å, whereas no nOe was observed between the same set of protons in compound ***rac*-1h**. nOe buildup curves were obtained by irradiating the key target protons on both samples. An internuclear distance of 2.4 Å for the distance from H-6 to H-5 (nucleoside numbering) was used as a reference for the calculations. Data points from the integrated nOe peaks were all normalized to 100% inversion of the target before the distance calculation was carried out.

Single-Crystal X-ray Diffraction Analysis of *rac*-1h. $C_{11}H_{13}N_3O_3 \cdot H_2O$, fw = 253.26, triclinic P-1, a = 5.535(1) Å, b = 7.358(1) Å, c = 15.176(4) Å, V = 593.6(1) Å^3, Z = 2, ρ_{calcd} = 1.414 Mg/m^3, λ(Cu Kα) = 1.54178 Å, μ = 0.921 mm^{-1}, F(000) = 268, T = 293(2) K. A colorless 0.39 × 0.28 × 0.06-mm^3 crystal was used for data collection. The theta range for data collection was 2.97 to 66.59° with 3510 reflections collected. Additional information and tables of coordinates, bond distances and bond angles, and anisotropic thermal parameters have been deposited with the Crystallographic Data Centre, Cambridge, CB2, and 1EW, England.

Antiviral Activity in MT-2 and MT-4 Cells. MT-4 cells (3 × 10^4) were exposed to 100 $TCID_{50}$ of HIV-1_{LAI} and were cultured in the presence of ***rac*-1h** and AZT and used as a control. The EC_{50} values were determined using an MTT assay

on day 5 of the cultures. All assays were conducted in duplicate. MT-2 cells (2×10^3) were exposed to 100 $TCID_{50}$ of HIV-1_{LAI} and were cultured in the presence of ***rac*-1h** and AZT. The EC_{50} values were determined using an MTT assay on day 7 of the cultures. All assays were conducted in duplicate.

Inhibition of Wild-Type HIV-1 RT. The assay was done in duplicate as previously described.[16] Briefly, for each sample, 0.25 μg of single-stranded M13mp18 DNA (New England Biolabs) was hybridized to 0.5 μL of 1.0 OD260/mL −47 sequencing primer (New England Biolabs). The template primer was suspended in a solution containing 100.0 μL of 25 mM Tris (pH 8.0), 75 mM KCl, 8.0 mM $MgCl_2$, 100.0 μg/mL bovine serum albumin (BSA), 10.0 mM 3-[(3-cholamidopropyl)-dimethylammonio-]-1-propanesulfonate (CHAPS), 2.0 mM dithiothreitol, 10.0 μM each of dATP, dGTP, and dTTP, 5.0 μM dCTP, 2.0 μM [α-^{32}P] dCTP, and the indicated concentration of inhibitor. Extension was initiated by the addition of 1.0 μg of wild-type HIV-1 RT or RT-variant M184V. The mixture was incubated for 30 min at 37°, and the reaction was halted by the addition of 3 mL of 10% trichloroacetic acid (TCA). Precipitated DNA was collected by suction filtration through Whatman GF/C glass filters. The amount of incorporated radioactivity was determined by liquid scintillation counting. The amount of incorporated radioactivity in the absence of inhibitor was considered 100% activity. The amount of radioactivity incorporated in the presence of inhibitor was normalized to this value.

Acknowledgment. We thank Dr. James A. Kelley of the Laboratory of Medicinal Chemistry, NCI-Frederick, CCR, for mass spectral data. The help of Mr. David A. Luca, Mr. John R. Klose, and Dr. Gwendolyn N. Chmurny of the NMR Group, Laboratory of Proteomics and Analytical Technologies, SAIC Frederick, for 1D and 2D NMR experiments, structural minimizations, and peak assignments is gratefully acknowledged.

Supporting Information Available: For ***rac*-1h**, crystallographic data, atomic coordinates, bond lengths and angles, ansiotropic displacement parameters, hydrogen coordinates and isotropic displacement parameters, torsion angles, hydrogen bonds, and a PDB file. This material is available free of charge via the Internet at http://pubs.acs.org.

References

(1) Ohrui, H.; Kohgo, S.; Kitano, K.; Sakata, S.; Kodama, E.; Yoshimura, K.; Matsuoka, M.; Shigeta, S.; Mitsuya, H. Syntheses of 4′−C-ethynyl-beta-D-arabino- and 4′−C-ethynyl-2′-deoxy-beta-D-ribo-pentofuranosylpyrimidines and -purines and evaluation of their anti-HIV activity. *J. Med. Chem.* **2000**, *43*, 4516−4525.

(2) Kodama, E. I.; Kohgo, S.; Kitano, K.; Machida, H.; Gatanaga, H.; Shigeta, S.; Matsuoka, M.; Ohrui, H.; Mitsuya, H. 4′-ethynyl nucleoside analogues: Potent inhibitors of multidrug-resistant human immunodeficiency virus variants in vitro. *Antimicrob. Agents Chemother.* **2001**, *45*, 1539−1546.

(3) Chen, M. S.; Suttmann, R. T.; Wu, J. C.; Prisbe, E. J. Metabolism of 4′-azidothymidine−A compound with potent and selective activity against the human immunodeficiency virus. *J. Biol. Chem.* **1992**, *267*, 257−260.

(4) Chen, M. S.; Suttmann, R. T.; Papp, E.; Cannon, P. D.; McRoberts, M. J.; Bach, C.; Copeland, W. C.; Wang, T. Selective action of 4′-azidothymidine triphosphate on reverse transcriptase of human immunodeficiency virus type-1 and human DNA polymerase-alpha and polymerase-beta. *Biochemistry* **1993**, *32*, 6002−6010.

(5) Oyang, C.; Wu, H. Y.; Frasersmith, E. B.; Walker, K. Synthesis of 4′-cyanothymidine and analogues as potent inhibitors of HIV. *Tetrahedron Lett.* **1992**, *33*, 37−40.

(6) Sugimoto, I.; Shuto, S.; Mori, S.; Shigeta, S.; Matsuda, A. Nucleosides and nucleotides. 183. Synthesis of 4′alpha- branched thymidines as a new type of antiviral agent. *Bioorg. Med. Chem. Lett.* **1999**, *9*, 385−388.

(7) Nomura, M.; Shuto, S.; Tanaka, M.; Sasaki, T.; Mori, S.; Shigeta, S.; Matsuda, A. Nucleosides and nucleotides. 185. Synthesis and biological activity of 4′-alpha-C-branched-chain sugar pyrimidine nucleosides. *J. Med. Chem.* **1999**, *42*, 2901−2908.

(8) Maag, H.; Rydzewski, R. M.; Mcroberts, M. J.; Crawfordruth, D.; Verheyden, J.; Prisbe, E. J. Synthesis and anti-HIV activity of 4′-azido- methoxynucleosides and 4′-methoxynucleosides. *J. Med. Chem.* **1992**, *35*, 1440−1451.

(9) Oyang, C.; Kurz, W.; Eugui, E. M.; McRoberts, M. J.; Verheyden, J.; Kurz, L. J.; Walker, K. 4′-Substituted nucleosides as inhibitors of HIV−An unusual oxetane derivative. *Tetrahedron Lett.* **1992**, *33*, 41−44.

(10) Lee, J.; Kang, J. H.; Lee, S. Y.; Han, K. C.; Torres, C. M.; Bhattacharyya, D. K.; Blumberg, P. M.; Marquez, V. E. Protein kinase C ligands based on tetrahydrofuran templates containing a new set of phorbol ester pharmacophores. *J. Med. Chem.* **1999**, *42*, 4129−4139.

(11) Ti, G. S.; Gaffney, B. L.; Jones, R. A. Transient protection: Efficient one-flask syntheses of protected deoxynucleosides. *J. Am. Chem. Soc.* **1982**, *104*, 1316−1319.

(12) Kang, J. H.; Siddiqui, M. A.; Lewin, N. E.; Pu, Y.; Sigano, D. M.; Blumberg, P. M.; Lee, J.; Marquez, V. E. Conformationally constrained analogues of diacylglycerol. 24. Asymmetric synthesis of a chiral (*R*)-DAG-lactone template as a versatile precursor for highly functionalized DAG-lactones. *Org. Lett.* **2004**, *6*, 2413−2416.

(13) Boyer, P. L.; Hughes, S. H. Analysis of mutations at position-184 in reverse-transcriptase of human-immunodeficiency-virus type-1. *Antimicrob. Agents Chemother.* **1995**, *39*, 1624−1628.

(14) Saraflanos, S. G.; Das, K.; Clark, A. D.; Ding, J. P.; Boyer, P. L.; Hughes, S. H.; Arnold, E. Lamivudine (3TC) resistance in HIV-1 reverse transcriptase involves steric hindrance with beta-branched amino acids. *Proc. Natl. Acad. Sci. U.S.A* **1999**, *96*, 10027−10032.

(15) Gao, H. Q.; Boyer, P. L.; Saraflanos, S. G.; Arnold, E.; Hughes, S. H. The role of steric hindrance in 3TC resistance of human immunodeficiency virus type-1 reverse transcriptase. *J. Mol. Biol.* **2000**, *300*, 403−418.

(16) Boyer, P. L.; Gao, H. Q.; Clark, P. K.; Saraflanos, S. G.; Arnold, E.; Hughes, S. H. YADD mutants of human immunodeficiency virus type 1 and Moloney murine leukemia virus reverse transcriptase are resistant to lamivudine triphosphate (3TCTP) in vitro. *J. Virol.* **2001**, *75*, 6321−6328.

(17) Gu, Z. X.; Qing, G.; Li, X. G.; Parniak, M. A.; Wainberg, M. A. Novel mutation in the human-immunodeficiency-virus type-1 reverse-transcriptase gene that encodes cross-resistance to 2′,3′-dideoxyinosine and 2′,3′-dideoxycytidine. *J. Virol* **1992**, *66*, 7128−7135.

(18) Tisdale, M.; Alnadaf, T.; Cousens, D. Combination of mutations in human immunodeficiency virus type 1 reverse transcriptase required for resistance to the carbocyclic nucleoside 1592U89. *Antimicrob. Agents Chemother.* **1997**, *41*, 1094−1098.

(19) Kohgo, S.; Mitsuya, H.; Ohrui, H. Synthesis of the L-enantiomer of 4′′−C-ethynyl-2′-deoxycytidine. *Biosci. Biotechnol. Biochem.* **2001**, *65*, 1879−1882.

(20) Haraguchi, K.; Takeda, S.; Tanaka, H.; Nitanda, T.; Baba, M.; Dutschman, G. E.; Cheng, Y. C. Synthesis of a highly active new anti-HIV agent 2′,3′-didehydro-3′-deoxy-4′-ethynylthymidine. *Bioorg. Med. Chem. Lett.* **2003**, *13*, 3775−3777.

(21) Choi, Y. S.; George, C.; Comin, M. J.; Barchi, J. J.; Kim, H. S.; Jacobson, K. A.; Balzarini, J.; Mitsuya, H.; Boyer, P. L.; Hughes, S. H.; Marquez, V. E. A conformationally locked analogue of the anti-HIV agent stavudine. An important correlation between pseudorotation and maximum amplitude. *J. Med. Chem.* **2003**, *46*, 3292−3299.

JM049550O

European Journal of Neuroscience, Vol. 19, pp. 2997–3005, 2004

Brain virus burden and indoleamine-2,3-dioxygenase expression during lentiviral infection of rhesus monkey are concomitantly lowered by 6-chloro-2′,3′-dideoxyguanosine

Candan Depboylu,[1,2] Todd A. Reinhart,[3] Osamu Takikawa,[4] Yoshinori Imai,[5] Hitomi Maeda,[6] Hiroaki Mitsuya,[6] Dianne Rausch,[7] Lee E. Eiden[7] and Eberhard Weihe[1]
[1]Department of Molecular Neuroscience, Institute of Anatomy and Cell Biology, Philipps University, Marburg, Germany
[2]Department of Neurology, Philipps University, Marburg, Germany
[3]Department of Infectious Diseases and Microbiology, University of Pittsburgh, Pittsburgh, USA
[4]Department of Molecular Biochemistry, Central Research Institute, School of Medicine, Hokkaido University, Sapporo, Japan
[5]Department of Neurochemistry, National Institute of Neuroscience, Tokyo, Japan
[6]Experimental Retrovirology Section, HIV and AIDS Malignancy Branch, Center for Clinical Research, NCI, NIH, Bethesda, USA
[7]Section on Molecular Neuroscience, Laboratory of Cellular and Molecular Regulation, NIMH, NIH, Bethesda, USA

Keywords: antiretroviral, kynurenine pathway, microglia/ macrophage, neuroinflammation, quinolinic acid

Abstract

Increased kynurenine pathway metabolism has been implicated in the aetiology of lentiviral encephalopathy. Indoleamine-2,3-dioxygenase (IDO) initiates the increased production of kynurenine pathway metabolites like quinolinic acid (QUIN). QUIN itself is elevated in AIDS-diseased monkey and human brain parenchyma and cerebrospinal fluid at levels excitotoxic for neurons *in vitro*. This study investigates the cellular origin of IDO biosynthesis in the brain of rhesus monkeys infected with simian immunodeficiency virus (SIV) and explores the effects of CNS-permeant antiretroviral treatment. IDO transcript and protein were absent from the brain of non-infected and SIV-infected asymptomatic monkeys. IDO biosynthesis was induced in the brain of monkeys exhibiting AIDS. Nodule and multinucleated giant cell-forming macrophages were the main sources of IDO synthesis. Treatment with the lipophilic 6-chloro-2′,3′-dideoxyguanosine suppressed IDO expression in the brain of AIDS-diseased monkeys. The effectiveness of this treatment was confirmed by the reduction of virus burden and SIV-induced perivascular infiltrates, mononuclear nodules and multinucleated giant cells. Our data demonstrate that brain IDO biosynthesis is induced in a subset of monocyte-derived cells, depends on viral burden and is susceptible to antiretroviral treatment. Thus, IDO induction is associated with reversible overt inflammatory events localized to areas of active viral replication in the SIV-infected brain.

Introduction

Macaques infected with simian immunodeficiency virus (SIV) develop cognitive and motor dysfunctions like human immunodeficiency virus (HIV)-infected individuals (Murray *et al.*, 1992). Impairments occur with low or marked encephalitis characterized by astrogliosis, nodule and giant cell formation, infiltrates, myelin pallor and vessel leakage (Budka, 1986; Lane *et al.*, 1986; Weihe *et al.*, 1993; Luabeya *et al.*, 2000). Loss of synapses, dendrites and neurons also occur in SIV disease (Luthert *et al.*, 1995; Li *et al.*, 1999; Bissel *et al.*, 2002). Neurodegenerative damage could be caused by virus-derived or host-derived neurotoxic products or by a combination of both (Lipton *et al.*, 1991; Li *et al.*, 1999), resulting in dementia in HIV-infected patients (Lawrence & Major, 2002). One of these host-generated toxins is quinolinic acid (QUIN). QUIN stimulates *N*-methyl-D-aspartate (NMDA)-type glutamate receptors (Perkins & Stone, 1983) and releases glutamate itself (Tavares *et al.*, 2002). QUIN elevation presumably contributes to altered neuronal activity (Abele *et al.*, 1990), neurodegeneration (Schwarcz *et al.*, 1983), other neurochemical alterations (Beal *et al.*, 1989) and astrogliosis (Block & Schwarz, 1994) in neuro-AIDS. Due to regional differences of NMDA-receptor distribution, some brain regions and neuronal populations are more vulnerable to the neurotoxic effect of QUIN than others (Schwarcz & Köhler, 1983).

The rate-limiting enzyme indoleamine-2,3-dioxygenase (IDO) catalyses the conversion of L-tryptophan into L-kynurenine. Subsequent enzymatic and non-enzymatic reactions convert L-kynurenine to QUIN. IDO is induced by cytokines, particularly interferon-γ released during systemic or brain inflammatory processes (Takikawa *et al.*, 1988; Dai & Gupta, 1990). Increased brain QUIN is directly related to IDO induction (Heyes *et al.*, 1988, 1989). It is hypothesized that QUIN in the brain comes from glial elements, endothelial cells, activated microglia and blood-derived macrophages (Brew *et al.*, 1995; Heyes *et al.*, 1997; Guillemin *et al.*, 1999; Hansen *et al.*, 2000). In the periphery, IDO was found to be expressed in dendritic cells and to influence lymphocyte function (Mellor *et al.*, 2002; Munn *et al.*, 2002). However, the sites of IDO expression during brain inflammation are not clearly identified in viral inflammatory diseases, limiting further understanding of the role of IDO-generated neurotoxins in neuro-AIDS and other neurodegenerative and neuroinflammatory diseases.

Correspondence: Dr E. Weihe, as above.
E-mail: weihe@staff.uni-marburg.de

Received 13 November 2003, revised 18 March 2004, accepted 19 March 2004

doi:10.1111/j.1460-9568.2004.03404.x

This study aims to determine if, where and how IDO is synthesized and regulated in SIV-induced brain inflammatory disease. Additionally, the influence of a lipophilic antiretroviral agent on brain IDO expression was analysed.

Materials and methods

Virus stock and inoculation procedures in rhesus monkeys

Juvenile rhesus macaques were housed in the BIOQUAL animal facility (Rockville, MD, USA), which is fully accredited by the American Association for Accreditation of Laboratory Animal Care. They were determined negative for simian retrovirus-1 and -2, SIV and simian herpes virus. Animals were inoculated intravenously with 10 rhesus infectious doses of cell-free SIV_{8B670} grown in human peripheral blood mononuclear cells. Virus was obtained as an aliquot of a previously characterized virus stock stored in liquid nitrogen (da Cunha *et al.*, 1995). Following inoculation, animals were monitored and examined for clinical evidence of disease. In short intervals blood and cerebrospinal fluid (CSF) samples were obtained from the animals. At time of killing and necropsy eight macaques exhibited clinical signs of AIDS and five did not. AIDS-defining criteria included one or more of the following: loss of body weight over 10%, intractable diarrhoea/dehydration requiring fluid replacement, oral lesions/thrush and other opportunistic infections. Four age-matched non-infected macaques were used as controls. Experiments involving the use of rhesus macaques were approved by the Animal Care and Use Commitee of Bioqual, Inc., an NIH-approved and Association for Assessment and Accreditation of Laboratory Animal Care (AAALAC)-accredited research facility. All experiments were carried out using the ethical guidelines promulgated in the National Institutes of Health Guide for the Care and Use of Laboratory Animals.

Antiretroviral treatment

Four SIV-infected monkeys, in which the viral load was found to be >100,000 virions/mL in plasma and >100 virions/mL in CSF in more than two consecutive examinations underwent treatment with 2′,3′-dideoxyinosine (ddI) or 6-chloro-2′,3′-dideoxyguanosine (6-Cl-ddG) subcutaneously (Shirasaka *et al.*, 1990, 1991; Hawkins *et al.*, 1995), and were killed shortly thereafter. These monkeys developed signs of AIDS-defining criteria during the course of antiretroviral treatment until death. Three of these four monkeys (MO76, MO77 and MO91) received 10 mg/kg/day ddI for 3 weeks for clinical stabilization and then 75 mg/kg/day of 6-Cl-ddG for 6 weeks. The fourth monkey (MO89) received 6-Cl-ddG (200 mg/kg/day) for 3 weeks. The vehicle for ddI administration was phosphate-buffered saline (PBS) and for 6-Cl-ddG administration 70% propylene glycol/30% PBS.

Tissue preparation for histochemical analysis

Prior to killing, animals were anaesthetized with ketamine (20 mg/kg) and ketamine-acepromazine (10 mg/kg), then perfused transcardially in the following sequence: PBS, 1% formalin/PBS and 4% formalin/PBS. Tissue specimens were obtained at necropsy and immersion-fixed overnight in 4% paraformaldehyde/PBS. Some blocks were cryopreserved in 10–20% sucrose/PBS over 48 h and snap frozen in cooled isopentane. Some blocks were postfixed in Bouin–Hollande solution, followed by extensive washes in 70% 2-propanol, dehydration and processing for paraffin embedding.

Radioactive and non-radioactive in situ *hybridization (ISH) histochemistry*

[^{35}S]-UTP- and digoxigenin-UTP-labelled human specific sense and antisense orientated riboprobes were generated by *in vitro* transcription

TABLE 1. Compiled results at time of killing and necropsy

Monkey number	Duration of infection (months)	Drug treatment*	Brain SIV burden†	Degree of SIV-induced encephalitis‡	Brain IDO synthesis§	Clinical findings
44	Not infected	Not treated	–	–	–	No disease
50	Not infected	Not treated	–	–	–	No disease
69	Not infected	Not treated	–	–	–	No disease
87	Not infected	Not treated	–	–	–	No disease
75	2.5	Not treated	–	–	–	Asymptomatic
80	6.5	Not treated	–	–	–	Asymptomatic
85	4.5	Not treated	–	–	–	Asymptomatic
92	6.0	Not treated	–	–	–	Asymptomatic
93	4.5	Not treated	–	–	–	Asymptomatic
46	19.0	Not treated	+	+	+	Diarrhoea, mycotic infection, mass
71	6.5	Not treated	++	++	++	Diarrhoea, listless, rash
74	6.0	Not treated	+++	+++	++	Diarrhoea, anaemia, parasitic infection, LN atrophy
78	2.4	Not treated	+++	+++	+++	Diarrhoea, parasitic infection, pneumonitis
79	2.5	Not treated	+	+	+	Rash, heart murmur, LN atrophy
82	3.0	Not treated	+++	+++	+++	Diarrhoea, wasting
86	4.5	Not treated	+++	+++	++	Wasting, mass, thrush, colitis, LN atrophy
90	2.3	Not treated	++	++	++	Vomiting, wasting, tube feed
76	22.0	ddI/6-Cl-ddG	–	–	–	Wasting, diarrhoea, heart murmur, anaemia
77	4.0	ddI/6-Cl-ddG	+/–	+/–	+/–	Incontinence, wasting, diarrhoea
89	22.0	6-Cl-ddG	–	–	–	Anaemia, wasting, diarrhoea, lymphoma
91	6.1	ddI/6-Cl-ddG	–	–	–	Wasting, diarrhoea

*Treatment with ddI prior with the CNS-permeant 6-Cl-ddG; MO89 received only 6-Cl-ddG. †Detection of SIV env/pol by ISH; detection of SIV *gp120* by IHC. ‡SIV-induced mononuclear reactions monitored by IHC for Iba1, scoring was as: +++ for severe, ++ for moderate and + for mild SIV-induced encephalitis with appearance of macrophage nodules, mononuclear cell infiltrates, multinucleated giant cells, – for no SIV-induced encephalitis. §Detection of IDO mRNA by ISH and of IDO protein by IHC; IHC for SIV *gp120* and IDO as well as ISH for IDO and SIV were scored as: – (no immunoreactive cells or cells with more than background silver grains) to +++ (>100 immunoreactive cells or cells with significantly greater number of silver grains than background per mm^2); numbers are not specifically determined; sections from temporal cortex, hippocampus and basal ganglia were analysed and summarized. 6-Cl-ddG, 6-chloro-2′,3′-dideoxyguanosine; ddI, 2′,3′-dideoxyinosine; IDO, indoleamine-2,3-dioxygenase; LN, lymph node; SIV, simian immunodeficiency virus.

from linearized pBluescript KS+ containing human IDO (accession no: M34455; kindly provided by S. L. Gupta, Hipple Cancer Research Center, Dayton, USA; Dai & Gupta, 1990) and alkaline hydrolysed to 200–250 nucleotide fragments prior to application. For prehybridization, frozen cryopreserved tissue sections (14 μm) were incubated in 10 mM Na-citrate buffer (pH 6.0) at 95 °C for 15 min, washed in PBS and in 0.4% Triton X-100/PBS for 10 min, acetylated with triethanolamine/acetic-anhydride (pH 8.0) for 10 min, rinsed in distilled water, dehydrated in graded ethanols, dried and used for hybridization, or stored at −20 °C until use. Hybridization with cRNA probes diluted in hybridization mix (final concentration of 50×10^3 d.p.m./μL for radioactive probe and 1 ng/μL for non-radioactive probe) overnight at 60 °C and post-hybridization were carried out as described previously (Schäfer *et al.*, 1992). Radioactive hybridization signals were revealed by autoradiography after 2–3 weeks of exposure on slides dipped in NTB-2 emulsion (Eastman Kodak, NY, USA). Non-radioactive hybridization signals were detected according to the manufacturer's instructions (Boehringer, Germany), resulting in a dark blue reaction product. ISH signals were analysed with the Olympus AX70 microscope (Olympus Optical, Germany). Sections from frontal cortex, parietal cortex, temporal cortex, occipital cortex, hippocampus, basal ganglia, thalamus, brainstem and spinal cord were analysed.

Single enzymatic immunohistochemistry (IHC)

As described previously (Weihe *et al.*, 1993), IHC was performed on deparaffinized paraffin-embedded tissue sections (7 μm) or cryosec-

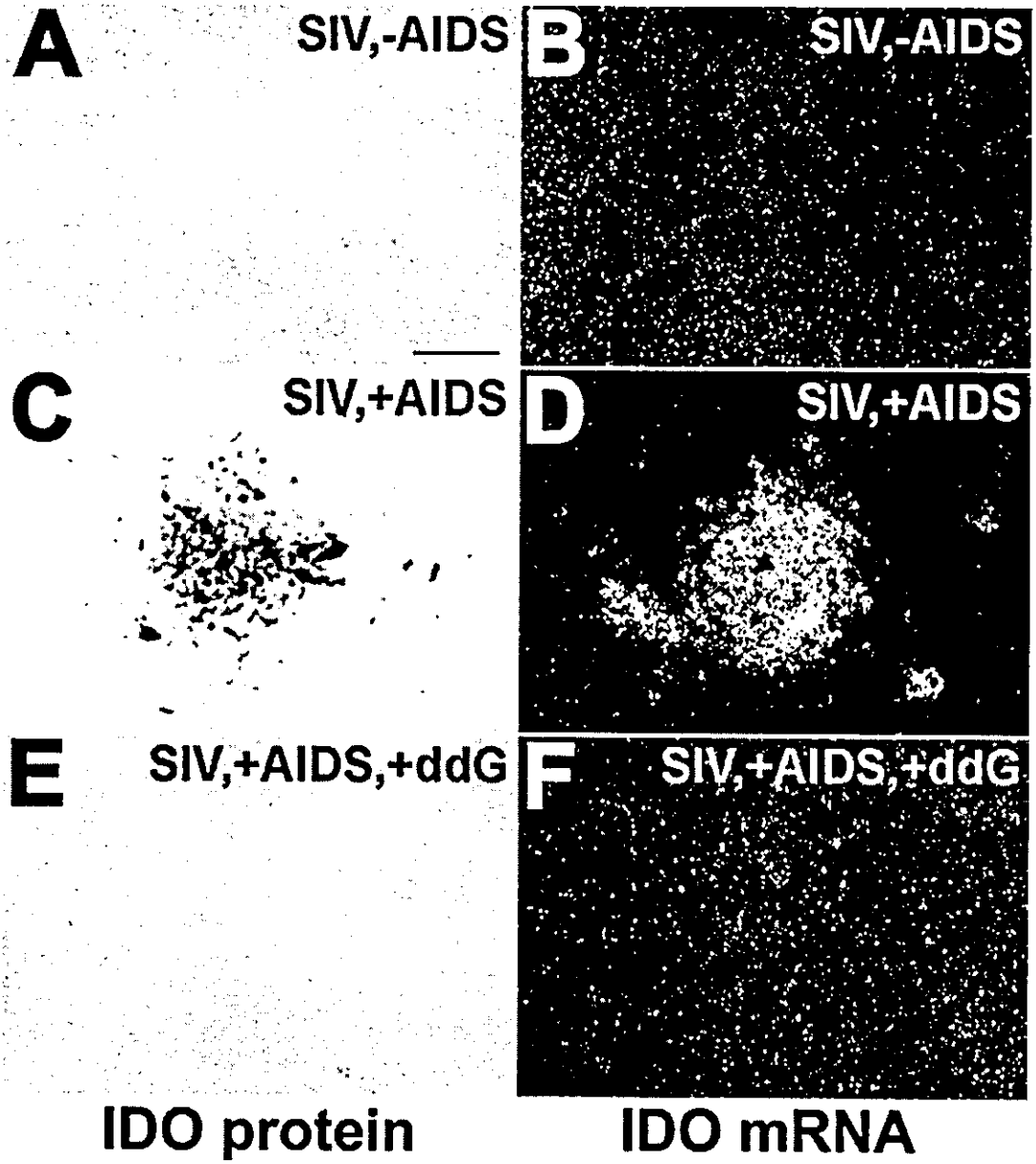

FIG. 1. Indoleamine-2,3-dioxygenase (IDO) biosynthesis in the rhesus monkey CNS in early and late stage of simian immunodeficiency virus (SIV) infection, and effect of antiretroviral treatment. (A, C and E) IHC for IDO protein, (B, D and F) ISH for IDO mRNA. (A and B) IDO protein and transcript are not detected in the brain of SIV-infected monkeys without AIDS (SIV, −AIDS). (C and D) In the brain of untreated SIV-infected monkeys with AIDS (SIV, +AIDS) IDO was induced. 6-Chloro-2′,3′-dideoxyguanosine (6-Cl-ddG) treatment (SIV, +AIDS, +ddG) inhibits expression of IDO protein and mRNA in the brain (E and F). Scale bar, 100 μm (A).

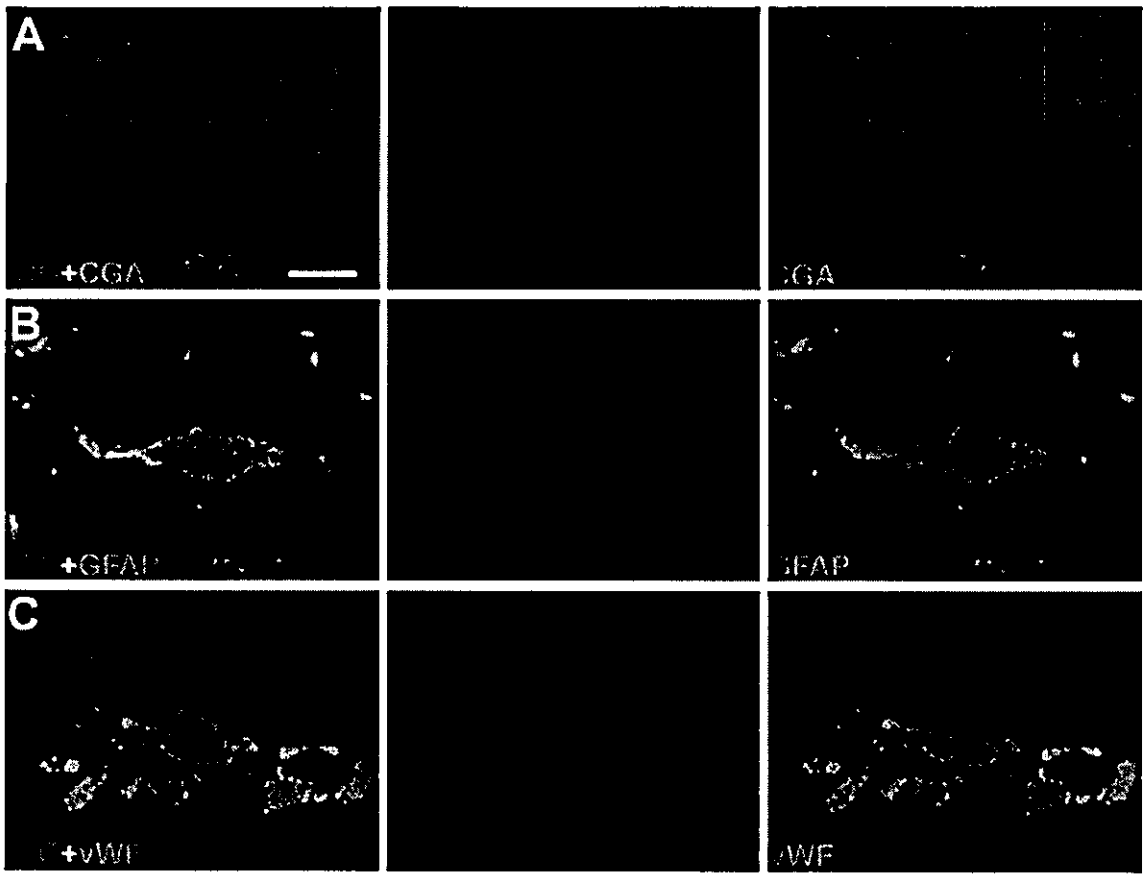

FIG. 2. Confocal laser scanning analysis after double immunofluorescence for IDO with established markers for brain resident cells demonstrates that chromogranin A (CGA)-positive neuronal cell bodies (A), glial fibrillary acid protein (GFAP)-positive astrocytes (B) and von Willebrand factor (vWF)-stained endothelial cells (C) are strictly lacking IDO in SIV encephalitis. Note vesicular appearance of IDO. Singular colours merged at A, B and C. Scale bar, 10 μm (A).

tions (14 μm) using standard avidin–biotin–peroxidase techniques (Vectastain Elite ABC kit, Boehringer). For optimal antigen retrieval, sections were incubated in a pressure cooker (15 min at 95 °C in 10 mM Na-citrate buffer, pH 6.0) and blocked by successive 30-min incubation in bovine serum albumin (BSA) and Avidin-Biotin-Blocking kit (Vectastain Elite, Boehringer). Cells of mononuclear origin were visualized with a rabbit-polyclonal antibody against ionized calcium-adapter binding molecule (Iba1; 1 : 3000; Imai *et al.*, 1996). IDO antigen was detected with a mouse-monoclonal antibody (1 : 400; Takikawa *et al.*, 1988). Primary antibodies were applied in 1%

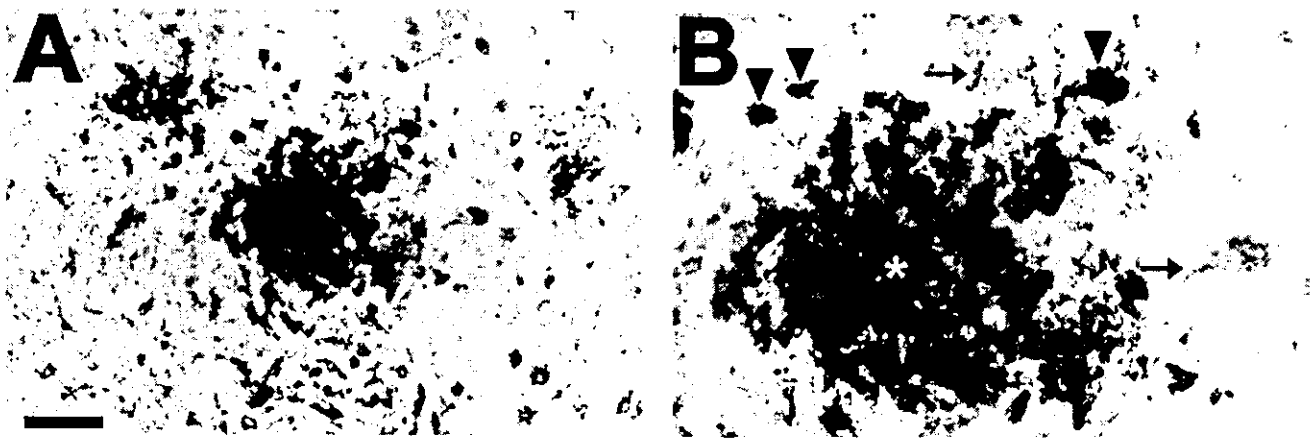

FIG. 3. Combination of non-radioactive ISH for IDO (dark blue reaction product) with cytochemistry for Iba1 (brown reaction product) on a brain section of an AIDS-diseased monkey. IDO mRNA is mainly localized in Iba1-positive macrophages and giant cell in the nodule (asterisk) but also in some Iba1-positive perinodular cells with mostly non-ramified appearance (arrow heads). Note also the presence of Iba1-positive cells with the appearance of ramified microglia, which are devoid of hybridization signals for IDO (arrows). Scale bar, 100 μm (for A); 50 μm (for B).

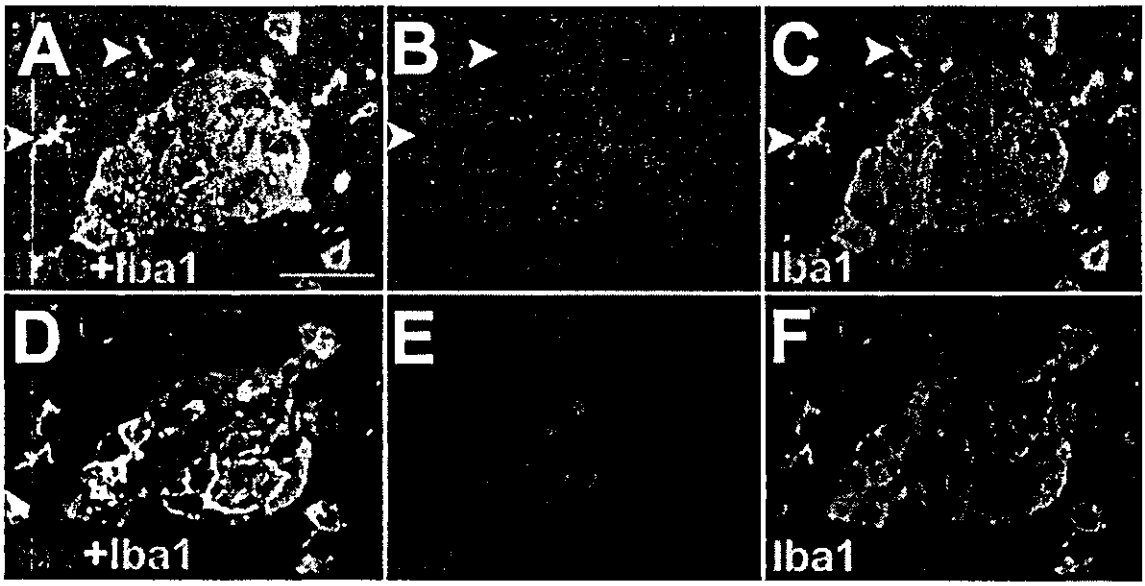

FIG. 4. Confocal double immunofluorescence of adjacent sections of a nodule from an AIDS-diseased monkey alternately stained for IDO with ionized calcium-adapter binding molecule (Iba1; A–C) and for SIV *gp120* with Iba1 (D–F), respectively. Note overlap of the distribution of IDO-positive and SIV-positive cells (B and E). Both IDO- and SIV-positive cells coincide with Iba1 within the nodule (C and F). Note distribution of Iba1 immunoreactivity to the surface of the nodular cells, while IDO and SIV immunoreactivities are localized to cell cytoplasm. Iba1-positive microglial cells in the perinodular region (arrow heads) lack immunoreactivity for IDO. Scale bar, 20 μm (A).

BSA/PBS and incubated at 16 °C overnight followed by 3 h at 37 °C. Sections were washed and incubated with species-specific biotinylated IgG from donkey (1 : 200; Dianova, Germany) for 1 h at 37 °C. Immunoreactions were visualized with 3,3′-diaminobenzidine (Sigma, Germany), resulting in a brown staining, or enhanced with 0.08% Nickel-salt (Fluka, Switzerland), resulting in a dark blue staining. IHC signals were analysed with the Olympus AX70 microscope (Olympus Optical).

Dual colour immunofluorescence and confocal laser scanning analysis

IDO and Iba1 were detected with the antibodies from mouse and rabbit at 1 : 40 and 1 : 300 dilutions, respectively. IDO was visualized by incubation with mouse-specific indocarbocyamine- or Alexa 647-conjugated IgG (1 : 100; Dianova), resulting in red-orange fluorescence labelling. Iba1 was detected after incubation with rabbit-specific biotinylated IgG and then with Alexa 488-conjugated streptavidin (1 : 200; MoBiTec, Germany), resulting in green fluorescence. The SIV_{8B670} was visualized with a cross-reacting mouse-monoclonal antibody KK45 against SIV_{mac251} glycoprotein 120 (*gp120*; 1 : 200; NIH AIDS Research & Reference Program, USA) and with Alexa 647-conjugated antimouse IgG (Kent *et al.*, 1992). Neurons were visualized with a rabbit-polyclonal antichromogranin A (CGA) antibody (1 : 1000; Schäfer *et al.*, 1994), endothelial cells with a rabbit-polyclonal anti-von Willebrand factor (vWF) antibody (1 : 500 diluted; DAKO, Germany; Theilen & Kuschinsky, 1992) and astrocytes with a polyclonal anti-glial fibrillary acid protein (GFAP) guinea pig-antibody (1 : 400; Progen, Germany; Weihe *et al.*, 1993). All three cell types were detected with Alexa 488-conjugated streptavidin after incubation with species-specific biotinylated IgG (1 : 200; Dianova). To make definitive statements of coexistence and non-coexistence pattern of IDO in neurons, astrocytes and endothelial cells in representative sections, containing hundreds to thousands of cells identified by the appropriate markers, we examined several sections (up to three) from several brain regions and for each untreated AIDS-diseased animal. Fluorescence signals were documented with the Olympus Fluoview confocal laser scanning microscope (Olympus Optical).

Combination of non-radioactive ISH with enzymatic IHC

For visualizing antigen with an RNA transcript in the same tissue section, IHC was performed in combination with ISH. Prehybridization, hybridization with the DIG-labelled probe against IDO mRNA and post-hybridization were performed as described. DIG-ISH signals

FIG. 5. Cells expressing IDO at the brain barrier of an untreated monkey with AIDS. (A and B) IDO transcript and protein-expressing monocytes (arrows) are attached to the endothelium surface. (C), IDO-positive multinucleated giant cell (arrow) is lying on the ependymal surface (ep). Scale bar, 12.5 μm (A).

for IDO mRNA were detected, resulting in a purple blue reaction product. After that Iba1 was visualized by 3,3′-diaminobenzidine-IHC as described, resulting in a brown reaction product. The reaction products could clearly be differentiated at the cellular level.

Detection of viral burden

For analysis of viral transcription, ISH was performed using probes generated by incorporation of [^{35}S] into SIV RNA probes by *in vitro* transcription of SIV_{mac239} sequences cloned in a pTRIKAN19 vector, or into DNA probes by random priming using sequences of cloned $SIV_{macBK28}$ DNA (Reinhart *et al.*, 1997). Activities of radioactive probes were $30–50 \times 10^3$ d.p.m./μL. The DNA templates were a *KpnI* fragment from the *pol* gene of SIV_{mac239} (nucleotide positions 5208–4713) or a *BamHI* fragment from $SIV_{macBK28}$ (nucleotide positions 1841–9174). In some experiments, ISH was performed with oligonucleotides specific for unspliced SIV RNA complementary to sequences at the exon/intron junction at the 5′-end of unspliced RNA (nucleotide positions 996–967of SIV_{smH4} proviral sequence) as described by Reinhart *et al.* (1997). The sequences in the control sense probe were identical to sequences at the same exon/intron junction (nucleotide positions 967–996 of SIV_{smH4}). Polyacrylamide gel-purified nucleotides were 3′-end-labelled with [^{35}S]-dCTP using terminal deoxynucleotide transferase to specific activities of $2–8 \times 10^9$ cpm/μg. For ISH, slide-mounted sections (14 μm) of cryo-preserved tissues were postfixed in 4% paraformaldehyde/PBS, washed and dehydrated. Pretreatments consisted of incubation for 20 min each in 0.2 N HCl at ambient temperature; 2 × SSC at 70 °C; and 2 mM $CaCl_2$, 20 mM Tris (pH 7.5) and 10 μg/mL proteinase K at 37 °C, followed by washing, acetylation and dehydration. Sections were then hybridized for 18 h at 45 °C (for riboprobes) or at 37 °C (for oligonucleotide probes). After post-hybridization sections were coated with NTB-2 emulsion and exposed at 4 °C for 3–6 days. After development, the sections were counterstained with cresyl violet. Sections from frontal cortex, parietal cortex, temporal cortex, hippocampus, basal ganglia, thalamus, brainstem and spinal cord were analysed.

Results

Analysis of IDO protein and transcript expression was performed on brain tissue sections of uninfected control monkeys (Ctrl), SIV-infected monkeys without AIDS (SIV, –AIDS) and SIV-infected monkeys exhibiting AIDS (SIV, +AIDS). A fourth group consisted of monkeys with high viremia and increased viral load in CSF at initiation of antiretroviral treatment and suffering from AIDS (SIV, +AIDS, +ddG). All animals are summarized in Table 1.

IDO is induced in the brain of SIV-infected monkeys exhibiting AIDS

IHC for IDO with a previously characterized mouse monoclonal antibody (Takikawa *et al.*, 1988) revealed no detectable staining in sections of different brain regions of control (not shown) and SIV-infected monkeys without symptoms of AIDS (Fig. 1A). In contrast, IDO protein was found to be expressed in the brain of monkeys exhibiting AIDS. This *de novo* expression was exclusively localized to non-neuronal cells in areas of infiltrates (Fig. 1C). To demonstrate that induced IDO expression depends on IDO gene transcription, ISH with [^{35}S]-labelled cRNA antisense probes was carried out. IDO mRNA was not detectable in brain tissue sections of control (not shown) and SIV-infected animals without AIDS (Fig. 1B). IDO mRNA was induced in the brain of SIV-infected monkeys with AIDS (Fig. 1D). The message exhibited a similar distribution pattern as protein in the brain.

Induction of IDO in the brain of AIDS-diseased monkeys occurs in a subset of monocyte-derived cell population in areas of virus burden

To identify the cells in which IDO is induced, co-staining experiments were performed on brain tissue sections of AIDS-diseased animals. High-power confocal laser scanning analysis after double immunofluorescence for IDO with established brain resident cellular markers CGA, GFAP and vWF revealed that neurons, astrocytes and endothelial cells did not express IDO (Fig. 2A–C). Oligodendrocytes, choroid plexus cells and ependymal cells did not synthesize IDO (not shown). A recently characterized marker known as Iba1 was used to identify the cells of monocytic origin including macrophages and microglia (Imai *et al.*, 1996). IDO biosynthesis was mainly found to be co-localized with Iba1 in and near areas of productive SIV infection, macrophage nodules and multinucleated giant cells (Figs 3A and B, and 4A–C). Confocal double immunofluorescence on adjacent sections demonstrated that IDO/Iba1-co-positive cells in nodules coincided with SIV *gp120*-positive cells co-stained for Iba1 or were in close proximity to them (Fig. 4D–F). In contrast, IDO was mostly absent from Iba1-positive ramified microglia (Fig. 4A–C).

Antiretroviral treatment reduces IDO induction in the brain

To determine the influence of viral transcription and translation on lentivirus-induced IDO biosynthesis, monkeys with high viremia and increased viral load in CSF were treated with ddI for clinical stabilization followed by lipophilic 6-Cl-ddG. Only one animal (MO89) was treated only with 6-Cl-ddG. The 6-Cl-ddG animals suffered from clinical symptoms of AIDS (SIV, +AIDS, +ddG). The biosynthesis of IDO in the brain was markedly reduced by the antiviral treatment (Fig. 1E and F), except in MO77, which showed some IDO synthesis albeit at very low levels (data not shown). The effectiveness of 6-Cl-ddG treatment on virus burden was monitored by SIV *gp120* immunostaining and by ISH for SIV transcripts. Viral burden as well as Iba1-positive mononuclear infiltrates, macrophage nodules and multinucleated giant cells were markedly reduced in the brain of 6-Cl-ddG-treated monkeys. Only in MO77 minor viral burden with some signs of productive inflammation was observed. The effects of antiviral treatment on IDO biosynthesis in relation to viral burden and mononuclear reactions in the brain are summarized in Table 1.

IDO is induced in monocytes at the blood–brain barrier in late stage of disease

The first sign of infiltration, the attachment of inflammatory cells on the endothelial surface, has been observed only in the brain of untreated AIDS-diseased monkeys. Some monocytes attached to endothelial cells expressed also IDO in the brain of AIDS-diseased monkeys (Fig. 5A and B), demonstrating IDO synthesis during infiltration through the blood–brain barrier. Apparently, these cells were truly adherent and in the progress of infiltrating into the brain as they were not washed away by the transcardial perfusion prior to or during fixation procedures. On the ventricular side there were also IDO-positive cells attached to ependymal surfaces (Fig. 5C). Both cellular phenomena were inhibited by 6-Cl-ddG.

Discussion

In this study we demonstrate that IDO was mainly induced in macrophages forming nodules and multinucleated giant cells and infiltrating monocytes in areas of SIV burden. IDO was mainly absent from diffusely distributed microglia. Induction of IDO in the brain was markedly suppressed by the treatment with 6-Cl-ddG.

The antiretroviral drug 6-Cl-ddG is a lipophilic prodrug of 2′,3′-dideoxyguanosine (Shirasaka *et al.*, 1990, 1991) and passes well through the blood–brain barrier of rhesus monkeys (Hawkins *et al.*, 1995). The administration of 6-Cl-ddG was found to effectively inhibit proliferation of HIV-1 (Shirasaka *et al.*, 1990, 1991) and SIV *in vitro* (Fujii *et al.*, 1998), and also primary proliferation of SIV in acutely infected rhesus monkeys (Fujii *et al.*, 1998). In chronically SIV-infected rhesus monkeys viral load in plasma and CSF decreased during 6-Cl-ddG treatment (Fujii *et al.*, 1997a). Moreover, a SIV-infected rhesus monkey with AIDS showed clinical signs of recovery during 6-Cl-ddG treatment (Fujii *et al.*, 1997b). Although our experimental design was different with treatment initiation at time of increased viral load in plasma and CSF (corresponding to 'virological AIDS'), our obtained results are quite consistent with the studies by Fujii *et al.* In 6-Cl-ddG-treated rhesus monkeys brain viral burden was markedly diminished, although the animals suffered from clinical symptoms of AIDS during treatment.

IDO can be activated in the brain following systemic immune stimulation with lipopolysacharide and in the course of inflammatory CNS diseases including HIV dementia (Sardar & Reynolds, 1995). Increased activity of the kynurenine pathway via IDO induction should produce high amounts of kynurenic acid and QUIN (Stone, 1993). While kynurenic acid may be neuroprotective, QUIN is a neurotoxin. In SIV/HIV-diseased subjects QUIN levels are elevated more than kynurenic acid levels in both brain parenchyma and CSF (Heyes *et al.*, 1989, 1990, 1998), suggesting a net neurotoxic effect of IDO induction.

Different cell types have been proposed as an intracerebral source of QUIN, among them endothelial cells, microglial cells, astrocytes and macrophages (Heyes *et al.*, 1997; Guillemin *et al.*, 1999; Hansen *et al.*, 2000), but direct co-localization studies of IDO and specific cellular markers have not been performed prior to the present study. Astrocytes and microglia can release QUIN *in vitro* (Heyes *et al.*, 1997; Guillemin *et al.*, 1999). CNS endothelial cells express IDO during malaria infection (Hansen *et al.*, 2000). Using high-resolution confocal double immunofluorescence and combination of ISH with IHC for IDO and specific cellular markers we have directly localized the site of IDO induction to cells in and near lesions containing cells with SIV, and not to other cellular loci of SIV-induced inflammation – resident microglia, astrocytes and endothelial cells – in which replicating virus is low or absent.

Interferon-γ is a potent inducer of IDO in macrophages (Takikawa *et al.*, 1999). IL-1 and TNFα, known to be elevated in the retroviral-infected brain (Benveniste, 1994), are also capable of stimulating IDO synthesis (Babcock & Carlin, 2000). Thus, SIV-induced IDO biosynthesis may be both initiated and sustained by these cytokines. IDO induction may be focused to areas of SIV-infected macrophages because these cytokines are uniquely present at these sites. It is also possible that locally produced virus particles may induce IDO. Marked differences in the regulation of IDO expression have been reported between macrophages and microglial cells (Alberati-Giani *et al.*, 1997). This may also explain why SIV-induced IDO biosynthesis was mainly localized to the macrophage/multinucleated giant cell compartment and did not occur globally in microglia in spite of synthesis of cytokines in both microglia and macrophages.

IDO localization to areas of virus replication implies that L-kynurenine generation is relatively focused, rather than globally activated, in the SIV-infected brain. IDO is not induced in bystander cells participating in generalized glial activation during CNS infection. As QUIN is a selective neurotoxin to cells bearing the NMDA-type glutamate receptor (Schwarcz *et al.*, 1983) – how does neurodegeneration during lentiviral infection originate from these foci of IDO production and spread diffusely throughout the brain? In part this may be due to the generation of highly diffusible substances from the sites of IDO production in the brain. Activation of IDO is functionally coupled to that of inducible nitric oxide synthase (iNOS; Alberati-Giani *et al.*, 1997) and iNOS is increased in areas of SIV replication (Li *et al.*, 1999). iNOS and IDO expression are both up-regulated by interferon-γ (Takikawa *et al.*, 1988; Melillo *et al.*, 1994). Expression of iNOS results in the generation of highly diffusible NO, which may synergize with QUIN to exacerbate neuronal damage. QUIN may be generated away from the sites of IDO production by diffusion of L-kynurenine into astrocytes and microglia that can convert it to QUIN (Heyes *et al.*, 1998). Finally, QUIN itself may release glutamate as a neurotoxin (Tavares *et al.*, 2002), further augmenting the wide-spread neurotoxic effect of QUIN.

Our obtained results are in concordance with a recently published study by Burudi *et al.* (2002), who reported that IDO mRNA expression occurred in cells of the monocytic lineage in SIV encephalitis, and that the levels of IDO mRNA correlated with viral load and interferon-γ levels. In addition, we demonstrated here that the expression and regulation of IDO mRNA was paralleled by the actual expression of IDO in the brain of SIV-infected monkeys. Our data indicate that the observed change in protein levels is likely occurring at the transcriptional level as a transcriptome response, rather than as a post-translational response. Our new finding that IDO production is susceptible to CNS-directed antiretroviral therapy correlating with decreased brain virus burden is consistent with reports of decreased QUIN levels in CSF of patients with AIDS following highly active antiretroviral therapy (Gendelman *et al.*, 1998; Look *et al.*, 2000). The effects of IDO and iNOS induction at local sites of SIV replication are likely to be transmitted globally to the brain, resulting in irreversible neurodegeneration, at some point in viral disease. Strategies for therapeutic intervention in neuro-AIDS may therefore need to take into account not only the effectiveness of blocking IDO and iNOS induction, but also the stage of disease at which their global effects are irreversibly transmitted from local sites of viral replication.

Acknowledgements

This study was supported by the Volkswagen Foundation to L. E. Eiden and E. Weihe. For excellent technical work we are indebted to R. Vertesi from L. E. Eiden's lab and E. Rodenberg-Frank, M. Zibuschka, P. Sack, P. Lattermann and H. Schneider from E. Weihe's lab. Parts of this study were presented at the Cojoint Meeting of the 4th International Symposium on Neurovirology and 10th Conference on Neuroscience on HIV Infection, June 2002, Düsseldorf, Germany.

Abbreviations

6-Cl-ddG, 6-chloro-2′,3′-dideoxyguanosine; BSA, bovine serum albumin; CGA, chromogranin A; CSF, cerebrospinal fluid; ddI, 2′,3′-dideoxyinosine; GFAP, glial fibrillary acid protein; *gp120*, glycoprotein *120*; HIV, human immunodeficiency virus; Iba1, ionized calcium-adapter binding molecule; IDO, indoleamine-2,3-dioxygenase; IHC, immunohistochemistry; iNOS, inducible nitric oxide synthase; ISH, *in situ* hybridization; NMDA, *N*-methyl-D-aspartate; PBS, phosphate-buffered saline; QUIN, quinolinic acid; SIV, simian immunodeficiency virus; vWF, von Willebrand factor.

References

Abele, A.E., Scholz, K.P., Scholz, W.K. & Miller, R.J. (1990) Excitotoxicity induced by enhanced excitatory neurotransmission in cultured hippocampal pyramidal neurons. *Neuron*, **2**, 413–419.

Alberati-Giani, D., Malherbe, P., Ricciardi-Castagnoli, P., Kohler, C., Denis-Donini, S. & Cesura, A.M. (1997) Differential regulation of indoleamine 2,3-dioxygenase expression by nitric oxide and inflammatory mediators in

IFN-gamma-activated murine macrophages and microglial cells. *J. Immunol.*, 159, 419–426.
Babcock, T.A. & Carlin, J.M. (2000) Transcriptional activation of indoleamine dioxygenase by interleukin 1 and tumor necrosis factor alpha in interferon-treated epithelial cells. *Cytokine*, **12**, 588–594.
Beal, M.F., Kowall, N.W., Swartz, K.J., Ferrante, R.J. & Martin, J.B. (1989) Differential sparing of somatostatin-neuropeptide Y and cholinergic neurons following striatal excitotoxin lesions. *Synapse*, **3**, 38–47.
Benveniste, E.N. (1994) Cytokine circuits in brain. Implications for AIDS dementia complex. *Res. Publishers Assoc. Res. Nerv. Ment.*, **72**, 71–88.
Bissel, S.J., Wang, G., Ghosh, M., Reinhart, T.A., Capuano, S. 3rd, Stefano Cole, K., Murphey-Corb, M., Piatak, M. Jr, Lifson, J.D. & Wiley, C.A. (2002) Macrophages relate presynaptic and postsynaptic damage in simian immunodeficiency virus encephalitis. *Am. J. Pathol.*, **160**, 927–941.
Block, F. & Schwarz, M. (1994) Expression of GFAP in the striatum and its projection areas in response to striatal quinolinic acid lesion in rats. *Neuroreport*, **5**, 2237–2240.
Brew, B.J., Corbeil, J., Pemberton, L., Evans, L., Saito, K., Penny, R., Cooper, D.A. & Heyes, M.P. (1995) Quinolinic acid production is related to macrophage tropic isolates. *J. Neurovirol.*, **1**, 369–374.
Budka, H. (1986) Multinucleated giant cells in the brain: a hallmark of the acquired immunodeficiency syndrome (AIDS). *Acta Neuropathol. (Berl.)*, **69**, 253–256.
Burudi, E.M., Marcondes, M.C., Watry, D.D., Zandonatti, M., Taffe, M.A. & Fox, H.S. (2002) Regulation of indoleamine 2,3-dioxygenase expression in simian immunodeficiency virus-infected monkey brains. *J. Virol.*, **76**, 12233–12241.
da Cunha, A., Rausch, D.M. & Eiden, L.E. (1995) An early increase in somatostatin mRNA expression in the frontal cortex of rhesus monkeys infected with simian immunodeficiency virus. *Proc. Natl. Acad. Sci. USA*, **92**, 1371–1375.
Dai, W. & Gupta, S.L. (1990) Molecular cloning, sequencing and expression of human interferon-γ-inducible indoleamine-2,3-dioxygenase cDNA. *Biochem. Biophys. Res. Commun.*, **168**, 1–8.
Fujii, Y., Mukai, R., Akari, H., Machida, M., Mori, K., Takasaka, M., Kojima, E., Murakami, K. & Yoshikawa, Y. (1998) Antiviral effects of 6-chloro-2′,3′-dideoxyguanosine in rhesus monkeys acutely infected with simian immunodeficiency virus. *Antivir. Chem. Chemother.*, **9**, 85–92.
Fujii, Y., Mukai, R., Mori, K., Akari, H., Otani, I., Ono, F., Kojima, E., Takasaka, M., Machida, M., Murakami, K. & Yoshikawa, Y. (1997a) Efficacy of 6-chloro-2′,3′-dideoxyguanosine (6-Cl-ddG) on rhesus macaque monkeys chronically infected with simian immunodeficiency virus (SIVmac239). *J. Acquir. Immune Defic. Syndr. Hum. Retrovirol.*, **16**, 313–317.
Fujii, Y., Mukai, R., Murayama, Y., Akari, H., Machida, M., Mori, K., Takasaka, M., Murakami, K. & Yoshikawa, Y. (1997b) Efficacy of 6-chloro-2′,3′-dideoxyguanosine (6-Cl-ddG) on an ARC/AIDS rhesus macaque (Macaca mulatta) infected with simian immunodeficiency virus. *Exp. Anim.*, **46**, 83–87.
Gendelman, H.E., Zheng, J., Coulter, C.L., Ghorpade, A., Che, M., Thylin, M., Rubocki, R., Persidsky, Y., Hahn, F., Reinhard, J. Jr & Swindells, S. (1998) Suppression of inflammatory neurotoxins by highly active antiretroviral therapy in human immunodeficiency virus-associated dementia. *J. Infect. Dis.*, **178**, 1000–1007.
Guillemin, G.J., Kerr, S.J., Smythe, G.A., Armati, P.J. & Brew, B.J. (1999) Kynurenine pathway metabolism in human astrocytes. *Adv. Exp. Med. Biol.*, **467**, 125–131.
Hansen, A.M., Driussi, C., Turner, V., Takikawa, O. & Hunt, N.H. (2000) Tissue distribution of indoleamine-2,3-dioxygenase in normal and malaria-infected tissue. *Redox Report*, **5**, 112–115.
Hawkins, M.E., Mitsuya, H., McCully, C.L., Godwin, K., Murakami, K., Poplack, D.G. & Balis, F.M. (1995) Plasma and cerebrospinal fluid pharmacokinetics of dideoxypurine nucleoside analogs in rhesus monkeys. *Antimicrob. Agents Chemother.*, **39**, 1259–1264.
Heyes, M.P., Kim, P. & Markey, S.P. (1988) Systemic lipopolysaccharide and pokeweek mitogen increase quinolinic acid content of mouse cerebral cortex. *J. Neurochem.*, **51**, 1946–1948.
Heyes, M.P., Mefford, I.N., Quearry, B.J., Dedhia, M. & Lackner, A. (1990) Increased ratio of quinolinic acid to kynurenic acid in cerebrospinal fluid of D-retrovirus *Rhesus macaques*: relationship to clinical and viral status. *Ann. Neurol.*, **27**, 666–675.
Heyes, M.P., Rubinow, D., Lane, C. & Markey, S.P. (1989) Cerebrospinal fluid quinolinic acid concentrations are increased in acquired immunodeficiency syndrome. *Ann. Neurol.*, **26**, 275–277.
Heyes, M.P., Saito, K., Chen, C.T., Proescholdt, M.G., Nowak, T.S. Jr, Li, J., Beagles, K.E., Proescholdt, M.A., Zito, M.A., Kawai, K. & Markey, S.P. (1997) Species heterogeneity between gerbils and rats: quinolinate production by microglia and astrocytes and accumulations in response to ischemic brain injury and systemic immune activation. *J. Neurochem.*, **69**, 1519–1529.
Heyes, M.P., Saito, K., Lackner, A., Wiley, C.A., Achim, C.L. & Markey, S.P. (1998) Sources of the neurotoxin quinolinic acid in the brain of HIV-1 infected patients and retrovirus-infected macaques. *FASEB J.*, **12**, 881–896.
Imai, Y., Ibata, I., Ito, D., Ohsawa, K. & Kohsaka, S. (1996) A novel gene iba1 in the major histocompatibiliy complex class III region encoding an EF hand protein expressed in a monocytic lineage. *Biochem. Biophys. Res. Commun.*, **224**, 855–862.
Kent, K.A., Rud, E., Cororan, T., Powell, C., Thiriart, C., Collignon, C. & Stott, E.J. (1992) Identification of two neutralizing and eight nonneutralizing epitopes on simian immunodeficiency virus envelope using monoclonal antibodies. *AIDS Res. Hum. Retroviruses*, **8**, 1147–1151.
Lane, J.H., Sasseville, V.G., Smith, M.O., Vogel, P., Pauley, D.R., Heyes, M.P. & Lackner, A.A. (1986) Neuroinvasion by simian immunodeficiency virus coincides with increased numbers of perivascular macrophages/microglia and intrathekal immune activation. *J. Neurovirol.*, **2**, 423–432.
Lawrence, E.M. & Major, E.O. (2002) HIV-1 and the brain: connections between HIV-1 associated dementia, neuropathology and neuroimmunology. *Mikrobes Infect.*, **4**, 301–308.
Li, Q., Eiden, L.E., Cavert, W., Reinhart, T.A., Rausch, D.M., Murray, E.A., Weihe, E. & Haase, A.T. (1999) Increased expression of nitric oxide synthase and dendritic injury in simian immunodeficiency virus encephalitis. *J. Human Virol.*, **2**, 139–145.
Lipton, S.A., Sucher, N.J., Kaiser, P.K. & Dreyer, E.B. (1991) Synergistic effects of HIV coat protein and NMDA receptor-mediated neurotoxicity. *Neuron*, **7**, 111–118.
Look, M.P., Altfeld, M., Kreuzer, K.A., Riezler, R., Stabler, S.P., Allen, R.H., Sauerbruch, T. & Rockstroh, J.K. (2000) Parallel decrease in neurotoxin quinolinic acid and soluble tumor necrosis factor receptor p75 in serum during highly active antiretroviral therapy of HIV type 1 disease. *AIDS Res. Human Retroviruses*, **16**, 1215–1221.
Luabeya, M.-K., Dallasta, L.M., Achim, C.L., Pauza, C.D. & Hamilton, R.L. (2000) Blood–brain barrier disruption in simian immunodeficiency virus encephalitis. *Neuropathol. Appl. Neurobiol.*, **26**, 454–462.
Luthert, P.J., Montgomery, M.M., Dean, A.F., Cook, R.W., Baskerville, A. & Lantos, P.L. (1995) Hippocampal neuronal atrophy occurs in rhesus macaques following infection with simian immunodeficiency virus. *Neuropathol. Appl. Neurobiol.*, **21**, 529–534.
Melillo, G., Cox, G.W., Biragyn, A., Sheffler, L.A. & Varesio, L. (1994) Regulation of nitric-oxide synthase mRNA expression by interferon-gamma and picolinic acid. *J. Biol. Chem.*, **269**, 8128–8133.
Mellor, A.L., Keskin, D.B., Johnson, T., Chandler, P. & Munn, D.H. (2002) Cells expressing indoleamine 2,3-dioxygenase inhibit T cell responses. *J. Immunol.*, **168**, 3771–3776.
Munn, D.H., Sharma, M.D., Lee, J.R., Jhaver, K.G., Johnson, T.S., Keskin, D.B., Marshall, B., Chandler, P., Antonia, S.J., Burgess, R., Slingluff, C.L. Jr & Mellor, A.L. (2002) Potential regulatory function of human dendritic cells expressing indoleamine 2,3-dioxygenase. *Science*, **297**, 1867–1870.
Murray, E.A., Rausch, D.M., Lendvay, J., Sharer, L.R. & Eiden, L.E. (1992) Cognitive and motor impairments associated with SIV infection in rhesus monkeys. *Science*, **255**, 1246–1249.
Perkins, M.N. & Stone, T.W. (1983) Pharmacology and regional variations of quinolinic acid-evoked excitations in the rat central nervous system. *J. Pharmacol. Exp. Ther.*, **226**, 551–557.
Reinhart, T.A., Rogan, M.J., Huddleston, D., Rausch, D.M., Eiden, L.E. & Haase, A.T. (1997) Simian immunodeficiency virus burden in tissues and cellular compartments during clinical latency and AIDS. *J. Infect. Dis.*, **176**, 1198–1208.
Sardar, A.M. & Reynolds, G.P. (1995) Frontal cortex indoleamine-2,3-dioxygenase activity is increased in HIV-1-associated dementia. *Neurosci. Lett.*, **187**, 9–12.
Schäfer, M.K.-H., Herman, J.P. & Watson, S.J. (1992) In situ hybridization immunohistochemistry. In London, E.D. (Ed), *Imaging Drug Action in the Brain*. CRC Press, Boca Raton, p. 337.
Schäfer, M.K.-H., Nohr, D., Romeo, H., Eiden, L.E. & Weihe, E. (1994) Panneuronal expression of chromogranin A in rat nervous system. *Peptides*, **15**, 263–279.
Schwarcz, R. & Köhler, C. (1983) Differential vulnerability of central neurons of the rat to quinolinic acid. *Neurosci. Lett.*, **38**, 85–90.